

**Water Resources Center  
Annual Technical Report  
FY 2015**

# Introduction

The Minnesota WRI program is a component of the University of Minnesota's Water Resources Center (WRC). The WRC is a collaborative enterprise supported by the College of Food, Agricultural, and Natural Resource Sciences (CFANS) and University of Minnesota Extension. The leadership of the center includes a Director, Jeff Peterson, who was hired in 2015, and an Associate Director, Faye Sleeper, who reports to the Director. The Director reports jointly to the Dean of CFANS and Dean of Extension. The previous leadership model included two co-Directors, Dr. Deborah Swackhamer and Faye Sleeper, who shared activities and responsibilities of administering its programs. After Deb Swackhamer retired as co-Director in 2014, Faye Sleeper served as Interim Director for one year.

## Research Program Introduction

The Call for Proposals for the FY15 WRRRI program was issued in September 2014. The WRC requested 3 to 5 external letter reviews for proposals received by the November deadline, drawing on reviewers from the University faculty, experts in the state, and experts from outside the state. Co-director Deborah Swackhamer convened an Advisory Council and they reviewed the proposals and their reviews, and made recommendations for funding based on the quality of the science, potential impact, potential for success, and external review comments. Seven proposals were received and three were funded. The projects receiving funding were all proposed by first-year, tenure-track faculty. Each project was featured in our quarterly newsletter, the Minnegram.

# Hydrogeochemical modeling of groundwater controls on sulfate and wild rice in streams

## Basic Information

|                                 |   |
|---------------------------------|---|
| <b>Title:</b>                   | Hydrogeochemical modeling of groundwater controls on sulfate and wild rice in streams |
| <b>Project Number:</b>          | 2015MN358B  |
| <b>Start Date:</b>              | 3/1/2015  |
| <b>End Date:</b>                | 2/28/2016   |
| <b>Funding Source:</b>          | 104B  |
| <b>Congressional District:</b>  | 5   |
| <b>Research Category:</b>       | Water Quality   |
| <b>Focus Category:</b>          | Hydrogeochemistry, Water Quality, Groundwater   |
| <b>Descriptors:</b>             | None  |
| <b>Principal Investigators:</b> | GeneHua Crystal Ng, Amy Elanor Myrbo  |

## Publications

1. Ng, G.-H.C., A.R. Yourd, A. Myrbo and N. Johnson. 2015. "Effects of Physical and Biogeochemical Processes on Aquatic Ecosystems at the Groundwater-Surface Water Interface: Evaluation of a Sulfate-impacted Wild Rice Stream in Minnesota" (oral presentation). AGU Fall Meeting 2015, San Francisco, CA.
2. Ng, G.-H.C. 2016. "Field Applications of Hydrogeochemical Modeling: What We Can Learn about Complex Interactions among Transport, Geochemistry, and Biology." St. Anthony Falls Laboratory, University of Minnesota.
3. Ng, G.-H.C. 2016. "Field Applications of Hydrogeochemical Modeling: What We Can Learn about Complex Interactions among Transport, Geochemistry, and Biology." Department of Geosciences seminar, University of Wisconsin - Madison, 1/21/16.
4. Ng, G.-H.C. 2016. "Modeling Sulfate in Groundwater on the Iron Range (NE Minnesota): Implications for Wild Rice." Environmental Engineering seminar, Department of Civil, Environmental and Geo-Engineering, University of Minnesota – Twin Cities. 4/22/16.
5. Yourd, A.R., G.-H.C. Ng, A. Myrbo and N. Johnson. 2015. "Surface Water, Groundwater, and Hyporheic Processes at Second Creek." DNR/MPCA Brown Bag Lunch Seminar, St. Paul, MN, 11/16/15.
6. Yourd, A.R., G.-H.C. Ng, A. Myrbo and N. Johnson. 2016. "Reactive Transport Modeling of Second Creek: a Mining Impacted Wild Rice Stream in Northeastern MN." Macalester GeoClub Lunch Seminar, St. Paul, MN, 2/24/16.
7. Yourd, A.R., G.-H.C. Ng, A. Myrbo and N. Johnson. 2016. "Wild Rice Root Zone Geochemistry," Soft Rock Lunch Seminar, Department of Earth Sciences, University of Minnesota – Twin Cities. 3/31/16.
8. Yourd, A.R., G.-H.C. Ng, A. Myrbo and N. Johnson. 2016. "Modeling Groundwater-Surface Water Interaction in a Mining Impacted Wild Rice Stream." Natural Resources Association of Graduate Students (NRAGS) Spring Symposium, University of Minnesota – Twin Cities, 4/15/16.
9. Yourd, A.R., G.-H.C. Ng, A. Myrbo and N. Johnson. 2016. "Modeling Groundwater-Surface Water Interaction in a Mining Impacted Wild Rice Stream," Earth Science Graduate Student Symposium, University of Minnesota – Twin Cities. 4/8/16.

## 1. Research

### i. Introduction / Background

The past few years have seen mounting questions regarding Minnesota's unique 10 mg/L sulfate standard in wild rice waters. This standard was established solely based on an empirical note in the 1940's that Minnesota lakes and streams with greater than 10mg/L sulfate generally lacked wild rice [Moyle, 1944]. The standard touches different interests in the state, including the economically important mining industry, which releases high concentrations of sulfate into surrounding watersheds, as well as native communities, whose right to access and harvest wild rice is federally protected by law. The state launched an intensive study over 2011 to 2013 on the connection between wild rice and sulfate. The study, led by the Minnesota Pollution Control Agency (MPCA), clarified much of the geochemical linkages, specifically finding that sulfide in the sediment porewater, not sulfate in the stream or lake, harms wild rice. Furthermore, factors such as organic carbon and iron abundance at a site affect whether sulfate produces significant levels of porewater sulfide. Our research follows on the heels of the MPCA study, and its start coincided with the MPCA's newly proposed site-specific porewater sulfide standard. While the proposed sulfide standard incorporates a regression-based formula that *statistically* interprets the MPCA's field data, our research seeks to provide a *process-based* understanding of unresolved aspects in the dataset. Such process-based understanding facilitates more robust water quality management, and it contributes to general scientific inquiry about complex hydrogeochemical processes affecting aquatic ecosystems.

Our research is motivated by the observation that streams sampled by the MPCA contained some of the highest concentrations of sulfate while still supporting healthy wild rice stands. Streams are more hydrologically dynamic than lakes, so porewater geochemistry can be influenced by both surface water and groundwater, depending on the hydrologic gradient. For example, in a gaining stream, low sulfate groundwater upwelling into the sediment porewater would not produce as much sulfide as down-welling high sulfate surface water. Although the effect of groundwater likely plays an important role in porewater geochemistry, especially in streams, groundwater flux or geochemistry was not studied as part of the MPCA research. Our research aims to incorporate groundwater data and groundwater-surface water interaction into the geochemical framework provided by the MPCA study. We use physical hydrology and geochemical field data collected during the summer of 2015 to inform a reactive transport model of a sulfate impacted wild rice stream in northeastern Minnesota. The model uses geochemical and hydrologic inputs to examine the effect of changing hydrologic regime on sediment porewater geochemistry over time.

### ii. Methods

#### *Study Area*

This research was conducted at Second Creek, a small stream catchment in the St. Louis River watershed in northeastern Minnesota (Figure 1). Second Creek is underlain by Quaternary glacial sediment and flows through a low-relief glacial outwash channel. The main channel of the stream (labeled "Second Creek" in Figure 2) is relatively narrow (2-3 m) and shallow (1-2 m), and it is flanked by 20-30 meters of wetlands (area from the channel to the trees in Figure 2). Wild rice is observed in the main channel of the stream during summer months, and the wetlands are highly vegetated with grasses, sedges, and shrubs. Water sources to Second Creek include mine tailings basin discharge, causing high sulfate levels in the main channel (>800 mg/L). Porewater iron levels are also unusually high (~40 mg/L), while porewater sulfide levels are low (~30 ug/L).

#### *Field Methods*

We collected physical and geochemical data from Second Creek from May through October in 2015. The goal of the physical hydrology measurements was to constrain regional groundwater flow and local groundwater-surface water interaction in the wetland and main channel. Figure 2 shows locations of groundwater monitoring wells and hand-installed mini piezometers used to track hydraulic head over

time. In early June, six groundwater wells were drilled and equipped with pressure transducers that recorded pressure and temperature at 10 minute intervals. Pressure transducers were also installed in four piezometers in the wetland and in a stream gauge in the main channel in order to track local hydraulic head conditions. Streambed flux was inferred from mini piezometers in the wetland and temperature probes in the main channel and wetland. Three vertical temperature probes were constructed using 1-inch diameter PVC tubing with a line of 6-8 thermistors affixed with epoxy. The probes were inserted into the stream or wetland sediment (Figure 3b) such that the top thermistor was approximately at the sediment-water interface; the bottom thermistor was located about 30-40cm depth, with most sensors clustered within the top 10 cm corresponding to the wild rice root zone. Temperature readings were logged at 1 minute to 15 minute intervals, adequately approximating continuous readings over the deployment period. Probes were deployed for 24-48 hours to capture a diurnal signal in the surface water boundary. Seepage meters were also deployed for 24-48 hours in the main channel and wetland to qualitatively measure flux direction (Figure 3a).

Geochemical data was collected on a monthly basis during the study period from groundwater, surface water, porewater, and streambed and wetland sediment. Groundwater and surface water data types included major cations and anions, alkalinity, pH, specific conductivity, and dissolved oxygen. Porewater data included cations, anions, alkalinity, sulfide, pH, and oxidation reduction potential. Cation samples were acidified with 1N HCl, sulfide samples were kept anoxic and preserved with ZnAc and NaOH, and porewater alkalinity samples were also preserved in an anoxic environment. Groundwater wells were sampled after three well volumes were pumped out of the well. Porewater samples were collected from the main channel and the wetland using a sediment gravity corer (Figure 3c). On shore, plastic wrap was placed on the top of the core to avoid oxygen intrusion; filters were then inserted into the top of the sediment core and attached to a septum bottle under a vacuum to collect the porewater sample (Figure 3d). Passive porewater equilibrators (“peepers”) were also used to sample porewater in late August (Figure 3e). Peepers allow for diffusion of porewater into wells spaced at 1.56 cm intervals, producing high vertical resolution geochemical profiles in the redox-sensitive porewater zone. Peepers were installed 2-3 week prior to collection in order to allow for adequate equilibration with surrounding porewater, and were sampled for pH, cations, anions, sulfide, and methane under a nitrogen atmosphere. Sediment samples were collected from the main channel and wetland and were analyzed for water content, total organic carbon, and acid volatile sulfide (AVS). AVS samples were collected under a nitrogen atmosphere, preserved with ZnAc, and frozen immediately upon collection.

### *Reactive Transport Model*

To investigate the role of groundwater on streambed geochemistry at Second Creek, we are using the 2015 field data together with the reactive-transport model PHT3D [Prommer et al., 2003], which combines modeled flow outputs generated by MODFLOW [Harbaugh 2005] together with the numerical transport method from the model MT3DMS [Zheng and Wang, 1999] and the geochemical capabilities of the PHREEQC-2 model [Parkhurst and Appelo, 1999]. The first step in the model implementation is to generate MODFLOW flow simulations based on hydrological conditions measured at the site. Focusing on our hypotheses regarding the control of groundwater upwelling versus downwelling, we cast the model domain as single vertical profiles that represent different locations and times within the streambed. Physical observations guided the specification of flux rates and magnitudes, and geochemical data served to further calibrate the values. The geochemical component of the model included the processes of kinetic anaerobic biodegradation of organic carbon coupled to Fe oxide and  $\text{SO}_4^{2-}$  reduction, precipitation of FeS and other Fe phases, and coupled carbonate and hydroxide chemistry. Field observations demonstrated the need to further include ion exchange and methanogenesis. Discrete simulation periods covering about a month at a time followed our sampling schedule. Initial concentration conditions for each simulation incorporated geochemical data from the corresponding sample time, and boundary conditions followed surface water and groundwater chemistry data. Porewater geochemical data collected at the end of the simulated period served as calibration points for estimating kinetic parameters and organic carbon concentrations.

### iii. Results and Discussion

#### a. Field results and discussion

##### *Physical Hydrology:*

Much of the physical hydrology at the site was dominated by an unusual prolonged flood event caused by the clogging of a culvert situated at the downstream end of the research area. As shown by the stream head time series in Figure 2, this began around 7/15/15 and ended around 9/25/15 with the clearing of the culvert. This event unfortunately washed out all the wild rice. However, it provided the unique opportunity of testing geochemical conditions under highly distinct hydrological conditions. Specifically, non-flood times could be candidates for gaining stream conditions, while the flood likely created losing conditions. Also, flood water filled the wetlands flanking the channel, essentially producing an on-site analogue to lake conditions that could be compared with the stream channel.

Continuous head measurements from the monitoring wells demonstrated the general groundwater flow field to travel from the west bank to the east bank over the summer (Figure 2), indicating that Second Creek may behave overall as a flow-through stream. Detailed estimates of streambed fluxes were more difficult to determine, because measurement errors masked small head gradient readings within the streambed, and methane bubbles hindered the operation of seepage meters. Qualitatively, the wetland piezometers and seepage meters indicated upward flux during non-flood periods and downward flux during the flood. Temperature probes produced the most robust flux estimates, yet they do so for very small spatial and temporal windows that may not provide a very general representation. Table 1 shows that during non-flood times, mostly upward flux was estimated for the western portion of the channel. Corroborating the idea of a flow-through system, downward to negligible flux were found in the mid- to east sections following the flood. However, contradicting the expected trend, we estimated upward flux throughout the flood period in the west-side wetland. Stream gauge data in Figure 2 show that these temperature probe measurements exactly coincided with two localized times of stream level drop within the flood period, which may have led to temporary reversals in flux direction. Also, the optimization analysis indicated flux direction to be less well-constrained during much of the flood time (Table 1).

Together, the physical hydrology data suggest that within a regional flow-through groundwater-stream system, non-flood periods were most likely to exhibit upwelling of groundwater, while the flooding facilitated downwelling. However, flux direction and magnitude were spatiotemporally variable within each period. This variability is characteristic of the hyporheic zone, the transition area between surface water and groundwater systems, and it complicates the physical and geochemical processes at this interface.

##### *Geochemistry:*

The approximately monthly geochemical sampling showed that upgradient (west-side) groundwater contains much lower sulfate concentrations compared to the surface stream water (Figure 4), which means that groundwater could buffer porewater concentrations in upwelling locations. This is reflected in the lower pre-flood sulfate concentrations in the (often gaining) west wetland and stream channel, compared to the flood time and to east-side locations. East-side porewater and groundwater concentrations show the influence of the surface water boundary conditions; this demonstrates the potential impact sulfate loading in surface systems may have on groundwater quality. Aqueous iron and sulfide measurements indicate active reduction of both iron and sulfate in the system. Peepers results in Figure 5 contained detailed information with depth and importantly provided a means for methane analysis. The flooded wetland, which serves as an analogue to a lake system, exhibited much more reducing conditions, as evidenced by the significant presence of methane.

#### b. Reactive-transport model results and discussion

Implementation of the reactive-transport model enabled integrated interpretation of the hydrological and geochemical data. Three preliminary simulation tests represented different hydrological scenarios: (1) losing (downward flux) stream channel, (2) gaining (upward flux) stream channel, and (3)

losing (downward flux) wetland (analogue for a lake setting). Multiple chemical components were included in the model; simulation profiles for key species are depicted in Figures 6a-c. Because the scope of our work extends beyond the specific features of Second Creek, the goal was not to perfectly match the data with the model. Instead, we aim to capture observed trends with the model. Simulations grounded to field data can then be analyzed to explore general processes that affect geochemical conditions in interacting groundwater-surface water systems.

For the losing (downward flux) channel, the simulation time period began with pre-flood July geochemical measurements, and the model was calibrated using pore water concentrations observed in September, which marks the end of the simulation (Figures 6a). Favorable comparison with the vertically resolved peeper data during the intermediary August time period lends confidence that key processes were adequately represented. Clearly, sulfate was transported into the streambed with downward advection over this time period. This is in great contrast to simulations for the gaining stream channel, in which high surface water sulfate concentrations negligibly penetrated the streambed (Figures 6b). Instead, with upward flux, the porewater profile was buffered by the much lower concentration groundwater sulfate. For both channel simulations, steady-state flux of  $o(10^{-8})$  m/s were determined through calibration, which are lower than the highest magnitude fluxes estimated with the temperature probes. This reflects the variable magnitude and direction flux within a non-flood or flood regime.

The last simulation test, the losing wetland, spanned July to August and shows an intermediary sulfate front travel depth compared to the first two simulations (Figures 6c). The losing wetland simulation differed from the others in a few key ways. Although both flood-period simulations should share the same surface water head conditions, fluxes in the wetland and channel could be distinct due to differences in both streambed head values and sediment hydraulic conductivity. In the wetland, finer sediment deposition in lower flow dynamics and higher organic matter content produce lower hydraulic conductivity. Correspondingly, the model calibration led to a lower magnitude flux in the wetland by an order of magnitude compared to the channel. Another distinction of the wetland is its more reducing conditions compared to the channel, which again relates to the high organic matter content. Constrained by methane concentrations found with the peepers, the wetland model required a significantly higher concentration of organic carbon than the channel model. Lake-beds are similar to wetlands in that they typically contain much greater amounts of organic matter compared to stream channels. Our model results show that that this leads to lower flux magnitudes and more reducing conditions, which limits sulfate transport into sediments and leads to high sulfate reduction activity.

A salient feature of all three simulation tests is the relatively low and similar porewater sulfide concentrations, which do not reach the 165 ug/L limit found by the MPCA to be harmful for wild rice. Low porewater sulfide concentrations are controlled by the precipitation of iron sulfide, which preliminary sediment extraction results show to be abundant. Thus, consistent with conclusions by the MPCA, iron precipitation ameliorates adverse effects of elevated sulfate concentrations. Simulations further reveal an important outcome. The wetland model, which serves as an analogue for lakes, precipitated about 10 times more iron sulfide over the same period as the stream channel. The MPCA database reveals that lake sites were far more likely to have lower porewater iron concentrations than streams, making them more susceptible to high sulfide levels. A possible explanation based on our simulations is that lakes with low iron concentrations may not be reflecting natural iron conditions, but they may have had reservoirs depleted by iron sulfide precipitation. Uncovering transient behavior highlights the importance of process understanding in the sulfate and wild rice problem.

#### iv. Preliminary Conclusions and On-going Work

Over the summer of 2015, we collected a diverse range of hydrological and geochemical data, covering the distinct components of a sulfate-impacted stream system: the stream surface water, porewater from the main channel and flanking wetlands, and the adjacent groundwater. The data were then integrated with a reactive-transport model to represent different hydrologic regimes defined by a major flood event. We have determined thus far that porewater geochemistry in streambeds depends not only on surface water but very much also on groundwater, with gaining stream conditions exhibiting more

buffered chemistry when groundwater concentrations of sulfate are low. However, groundwater flux can be highly variable in both magnitude and direction, which may attenuate the expected role of the surface or groundwater through reversing conditions. In addition to water chemistry, sediment geochemistry also strongly controls root zone geochemistry, with high organic carbon loads accelerating sulfate reduction, and iron reservoirs providing an important but finite sink for harmful sulfide.

Sediment analyses for organic carbon and sediment-associated iron will be completed within the next months and will provide additional model constraints that will improve our conceptual model of processes controlling the geochemistry at Second Creek. The transient behavior of the flow and geochemistry at the site has also sparked a new research collaboration at the site to investigate the microbial activity in highly dynamic and perturbed groundwater-surface water systems.

#### v. References:

- Harbaugh, AW (2005), MODFLOW-2005, The USGS modular ground-water model -- the Ground-Water Flow Process: USGS Techniques and Methods 6-A16, variously p.
- Moyle, J. (1944). Wild Rice in Minnesota. *The Journal of Wildlife Management*, 8(3), 177-184. doi:1. Retrieved from <http://www.jstor.org/stable/3795695> doi:1
- Parkhurst, DL, and CAJ Appelo. (1999) User's guide to PHREEQC: A computer program for speciation, reaction-path, ID-transport, and inverse geochemical calculations. USGS WR Inv Rep 99-4259.
- Prommer, H, DA Barry, and C Zheng (2003), MODFLOW/MT3DMS-Based Reactive Multicomponent Transport Modeling. *Groundwater*, 41: 247-257. doi: 10.1111/j.1745-6584.2003.tb02588.x
- Zheng, C, and PP Wang. (1999), MT3DMS: A modular three-dimensional multispecies model for simulation of advection, dispersion and chemical reactions of contaminants in groundwater systems: Documentation and user's guide. Contract Report SERDP-99-1. Vicksburg, Mississippi: U.S. Army Eng Res and Dev Center.

| <b>Dates</b>       | <b>location</b>   | <b>Flux [m/s]</b> | <b>MSE</b> | <b>direction</b> | <b>confidence in flow direction and magnitude</b> |
|--------------------|-------------------|-------------------|------------|------------------|---|
| <i>PRE-FLOOD:</i>  |                   |                   |            |                  |   |
| 6/6-6/7            | Mid-channel       | -1.26E-06         | 0.011      | up               | upward, magnitude moderately constrained          |
| 6/26-6/27          | West channel      | -1.23E-12         | 0.225      | up               | very confident close to 0                         |
|                    | Mid-Channel       | 9.88E-12          | 0.229      | down             | very confident close to 0                         |
| <i>FLOOD:</i>      |                   |                   |            |                  |   |
| 8/13-8/14          | West West-Wetland | -4.79E-06         | 0.023      | up               | upward, magnitude not well-constrained            |
|                    | Mid West-Wetland  | -5.91E-07         | 0.025      | up               | upward, magnitude not well-constrained            |
|                    | East West-Wetland | -1.50E-06         | 0.101      | up               | upward, magnitude moderately constrained          |
| 8/31-9/1           | West West-Wetland | -9.67E-06         | 0.041      | up               | upward, magnitude not well-constrained            |
|                    | Mid West-Wetland  | -9.88E-06         | 0.044      | up               | upward, magnitude not well-constrained            |
|                    | East West-Wetland | -6.62E-06         | 0.135      | up               | upward, magnitude not well-constrained            |
| <i>POST-FLOOD:</i> |                   |                   |            |                  |   |
| 10/16-10/17        | West channel      | -1.31E-06         | 0.029      | up               | upward, magnitude moderately constrained          |
|                    | Mid-Channel       | 4.17E-07          | 0.019      | down             | magnitude well-constrained, symmetric near 0      |
|                    | East channel      | -7.09E-12         | 1.447      | up               | 0 or upward                                       |

Table 1: Flux (positive downward) estimated by calibrating a 1D heat flow model to temperature probe time series data. Confidence in flux estimates was determined from the mean-square-error (MSE) (for the mismatch between model and observations) as a function of flux.

Figures

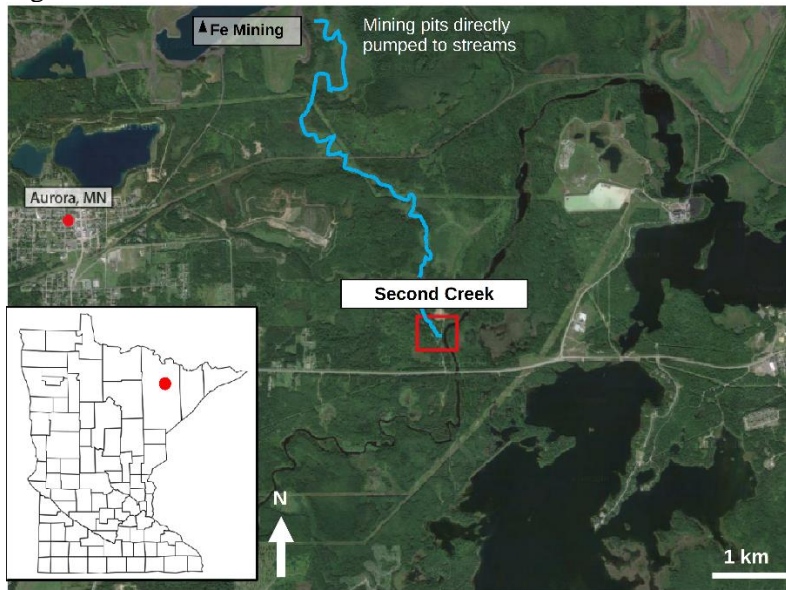


Figure 1: The Second Creek study site is located in northeast Minnesota, downgradient from taconite mining activity.

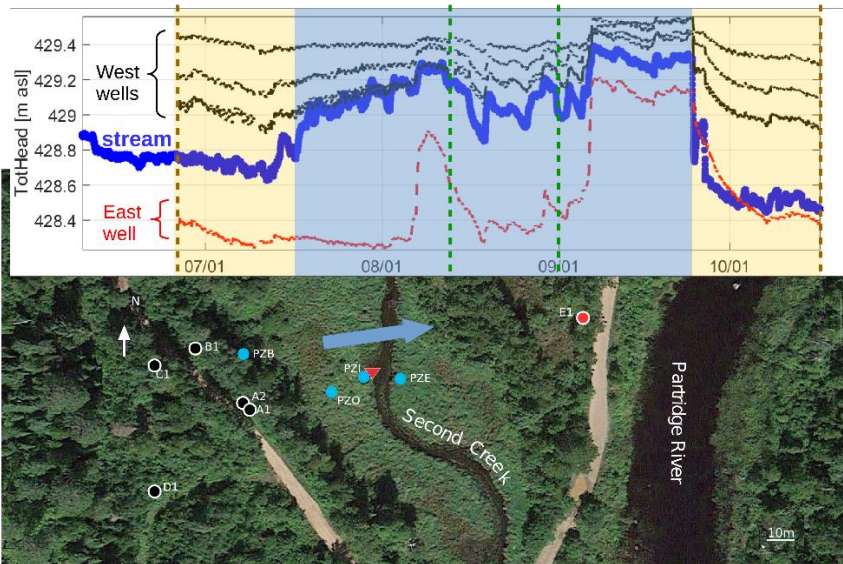


Figure 2: Lower: Location of groundwater monitoring wells (black and red circles) and wetland piezometers (light blue circles) at the field site (centrally marked by the red triangle). Upper: Head time series for the stream (thick blue line), west-side groundwater monitoring wells (black lines), and the east-side groundwater monitoring well (red line). Temperature probes were installed in the channel (wetland) during the times indicated with brown (green) dashed lines. Groundwater monitoring well and stream head data show a general west to east regional flow, likely resulting in a flow-through stream system. The flood period is highlighted in blue.



Figure 3: a) Seepage meter, b) Temperature probes, c) sediment gravity corer, d) apparatus for sampling porewater from core, e) “peeper”

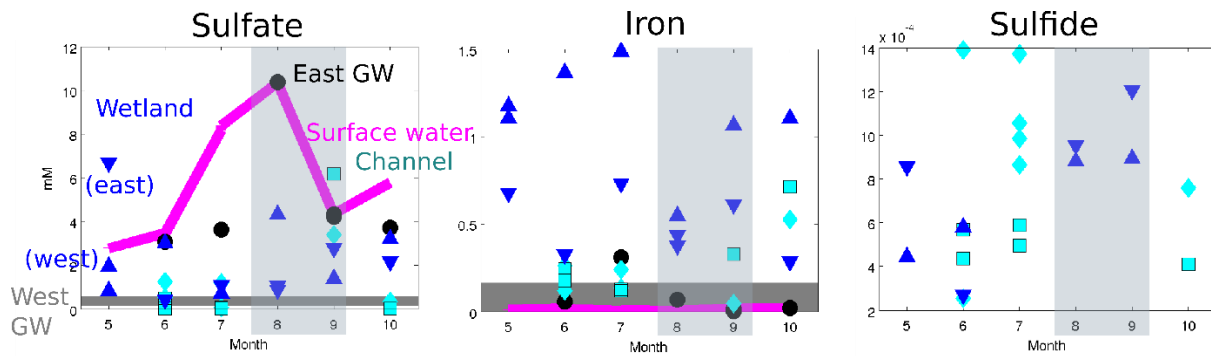


Figure 4: Porewater chemistry from each sampling month. Flood period shaded in gray. Surface water (magenta line) and west groundwater (gray strip), and east groundwater (black circle) represent the boundary conditions. Wetland (dark blue) and channel (light blue) conditions indicate the relative influence of the surface versus groundwater and the redox conditions.

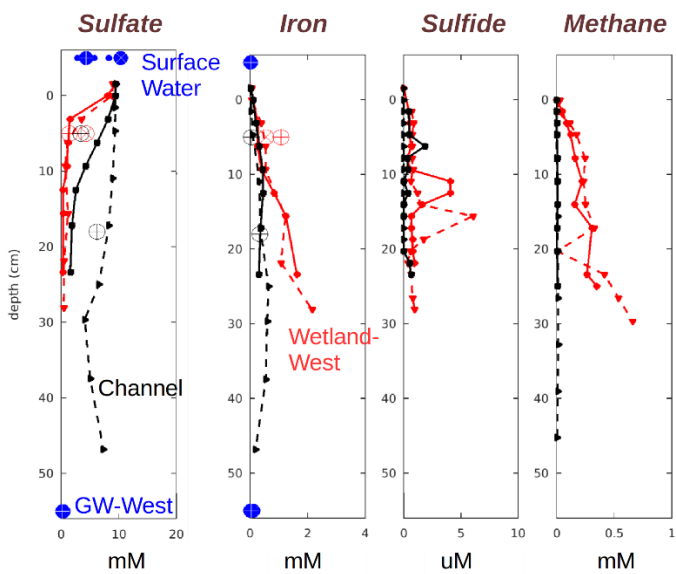


Figure 5: Peepers deployed over 8/15/15-9/1/15 (flood period) provide porewater concentration profiles at replicate channel (black) and west-wetland (red) locations. Note that one of the channel locations (dashed) likely consisted of localized sediment conditions that may not be highly representative of the surrounding area. Surface water and west-side groundwater conditions are shown for reference.

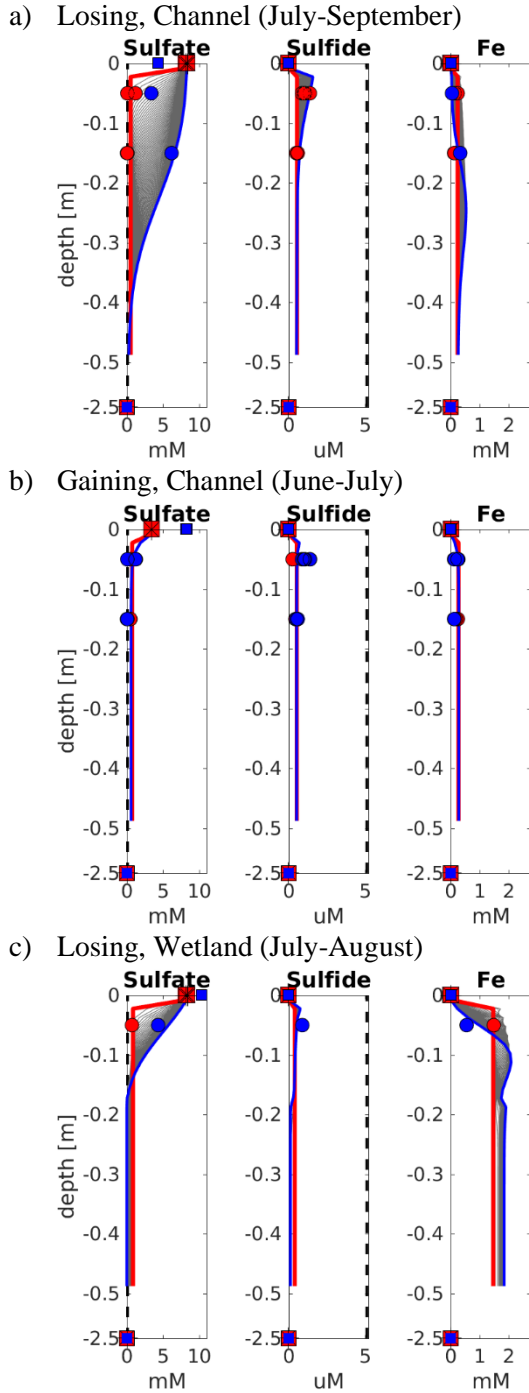


Figure 6: Simulated profiles (each line represents one day) are shown with observed concentrations (symbols). The start of the simulation period (red line) is initiated with corresponding porewater data (red circle), while the end time porewater data (blue circle) serve as calibration targets (blue line is simulated end profile). Surface water (depth=0) and groundwater (represented at depth = -2.5m) data (squares) serve as upper and lower boundary conditions.

## **2. Publications**

Ng, G.-H.C., A.R. Yourd, A. Myrbo and N. Johnson. 2015. "Effects of Physical and Biogeochemical Processes on Aquatic Ecosystems at the Groundwater-Surface Water Interface: Evaluation of a Sulfate-impacted Wild Rice Stream in Minnesota" (oral presentation). AGU Fall Meeting 2015, San Francisco, CA.

## **3. Student Support**

1 M.S. student, 1 Undergraduate student

## **4. Presentations**

Ng, G.-H.C. 2016. "Field Applications of Hydrogeochemical Modeling: What We Can Learn about Complex Interactions among Transport, Geochemistry, and Biology." St. Anthony Falls Laboratory, University of Minnesota.

Ng, G.-H.C. 2016. "Field Applications of Hydrogeochemical Modeling: What We Can Learn about Complex Interactions among Transport, Geochemistry, and Biology." Department of Geosciences seminar, University of Wisconsin - Madison, 1/21/16.

Ng, G.-H.C. 2016. "Modeling Sulfate in Groundwater on the Iron Range (NE Minnesota): Implications for Wild Rice." Environmental Engineering seminar, Department of Civil, Environmental and Geo-Engineering, University of Minnesota – Twin Cities. 4/22/16.

Yourd, A.R., G.-H.C. Ng, A. Myrbo and N. Johnson. 2015. "Surface Water, Groundwater, and Hyporheic Processes at Second Creek." DNR/MPCA Brown Bag Lunch Seminar, St. Paul, MN, 11/16/15.

Yourd, A.R., G.-H.C. Ng, A. Myrbo and N. Johnson. 2016. "Reactive Transport Modeling of Second Creek: a Mining Impacted Wild Rice Stream in Northeastern MN." Macalester GeoClub Lunch Seminar, St. Paul, MN, 2/24/16.

Yourd, A.R., G.-H.C. Ng, A. Myrbo and N. Johnson. 2016. "Wild Rice Root Zone Geochemistry," Soft Rock Lunch Seminar, Department of Earth Sciences, University of Minnesota – Twin Cities. 3/31/16.

Yourd, A.R., G.-H.C. Ng, A. Myrbo and N. Johnson. 2016. "Modeling Groundwater-Surface Water Interaction in a Mining Impacted Wild Rice Stream." Natural Resources Association of Graduate Students (NRAGS) Spring Symposium, University of Minnesota – Twin Cities, 4/15/16.

Yourd, A.R., G.-H.C. Ng, A. Myrbo and N. Johnson. 2016. "Modeling Groundwater-Surface Water Interaction in a Mining Impacted Wild Rice Stream," Earth Science Graduate Student Symposium, University of Minnesota – Twin Cities. 4/8/16.

# Invasive mussel shells and biogeochemistry of Minnesota lakes

## Basic Information

|                                 |   |
|---------------------------------|---|
| <b>Title:</b>                   | Invasive mussel shells and biogeochemistry of Minnesota lakes |
| <b>Project Number:</b>          | 2015MN360B  |
| <b>Start Date:</b>              | 3/1/2015  |
| <b>End Date:</b>                | 2/28/2016   |
| <b>Funding Source:</b>          | 104B  |
| <b>Congressional District:</b>  | 8th   |
| <b>Research Category:</b>       | Biological Sciences   |
| <b>Focus Category:</b>          | Invasive Species, Water Quality, Geochemical Processes        |
| <b>Descriptors:</b>             | None  |
| <b>Principal Investigators:</b> | Ted Ozersky   |

## Publications

There are no publications.

## Role of invasive mussel shell material in lake biogeochemistry

Ted Ozersky

1) Research:

### Study objectives:

Invasive dreissenid mussels (zebra and quagga mussels) are changing aquatic ecosystems throughout North America, with large and diverse effects on water quality, biological communities and productivity of invaded lakes and rivers. The ecological impacts of dreissenids are exerted through different mechanisms, including re-engineering of the cycling of ecologically important elements such as carbon, nitrogen and phosphorus. Dreissenids impact nutrients by removing particulate nutrients and carbon (phytoplankton and other suspended matter) from the water column; these elements can then have a number of fates: they can be excreted in dissolved form as metabolic wastes, deposited in solid form as feces or incorporated into tissue and shell material (Figure 1). While there is some information available about dreissenid nutrient excretion and soft tissue composition, there is little data about nutrients in dreissenid shells, the long term fate of shell material and how nutrient excretion, deposition and composition vary among different systems. This information is necessary in order to construct complete nutrient and carbon budgets for dreissenid populations in invaded lakes and understand how dreissenids impact lake ecosystems. **Our overall objective was to construct comprehensive nutrient budgets for dreissenid populations in MN lakes of varying nutrient status and size.** Specific objectives included: **a) quantifying the distribution and biomass of living dreissenids and discarded shell material in different lakes; b) assessing C, N and P concentrations in dreissenid tissues and the excretion and deposition rates of these elements in dissolved and solid form in different lakes c) determining potential environmental drivers of variation in composition and nutrient release d) measuring shell dissolution rates and return of elements bound in shells into nutrient cycling and e) constructing detailed nutrient budgets for dreissenids in different MN lakes.**

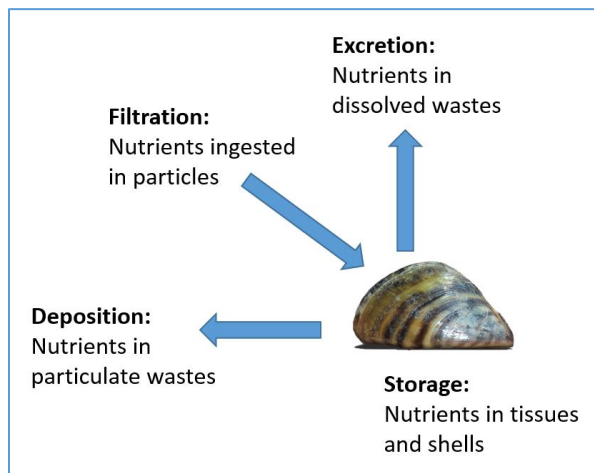


Figure 1: Nutrient budget of invasive dreissenid mussels

### Work performed:

WRC funding supported one summer field season of intensive sampling in 12 MN lakes (2015) and on-going sampling in 1 lake (Figure 2). Study lakes varied in size and trophic status. Summer sampling included characterization of water quality parameters in each lake, benthic sampling of dreissenid mussel populations for biomass and chemical composition determination across a depth gradient in 9 lakes, and deployment of shell dissolution experiments in 10 lakes. Benthic samples were analysed to determine tissue and shell biomass of living mussels and the mass of discarded shell material from dead mussels. Shells and soft tissues of different sized mussels from each lake were analysed for C, N and P

composition. On-going sampling in 1 lake (Pike Lake) was focused on determination of seasonal variability in dreissenid mussel tissue and shell C, N and P composition and secondary productivity rates. During the reporting period we analysed all mussel shell and tissue biomass samples and determined C, N, and P concentrations in mussels from 7 lakes.

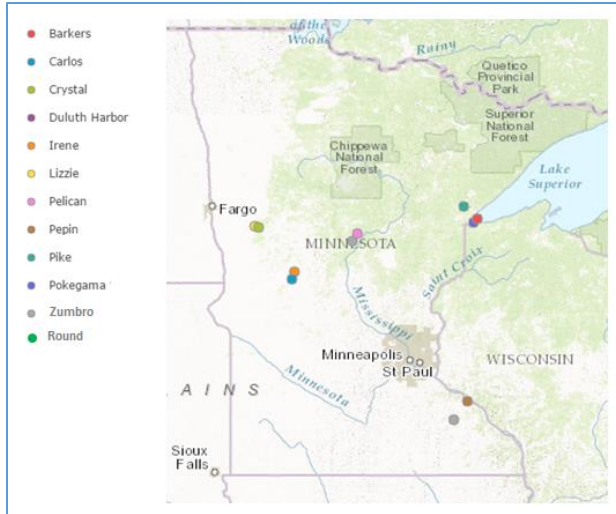


Figure 2: Map of sampling sites for biomass determination, nutrient measurements and shell dissolution experiments

## Results:

### Mussel biomass

Live mussel biomass was highly variable within and between lakes, ranging from 0 to a maximum of 43.3 g/m<sup>2</sup> for dry soft tissue biomass and 1,136 g/m<sup>2</sup> for live shell mass. Discarded shell mass was also highly variable and reached as high as 10,742 g/m<sup>2</sup>. Average biomass of live tissue, live shell and discarded shell biomass across all samples were 3.5 ±9.6 SD, 71.5±185.6 SD and 278.8±908.9 SD, respectively. Very little discarded shell and relatively few live mussels were found below depth of 6 m across the study lakes (Figure 3). There was no significant relationship between living mussel biomass and discarded shell mass across individual samples (Figure 4).

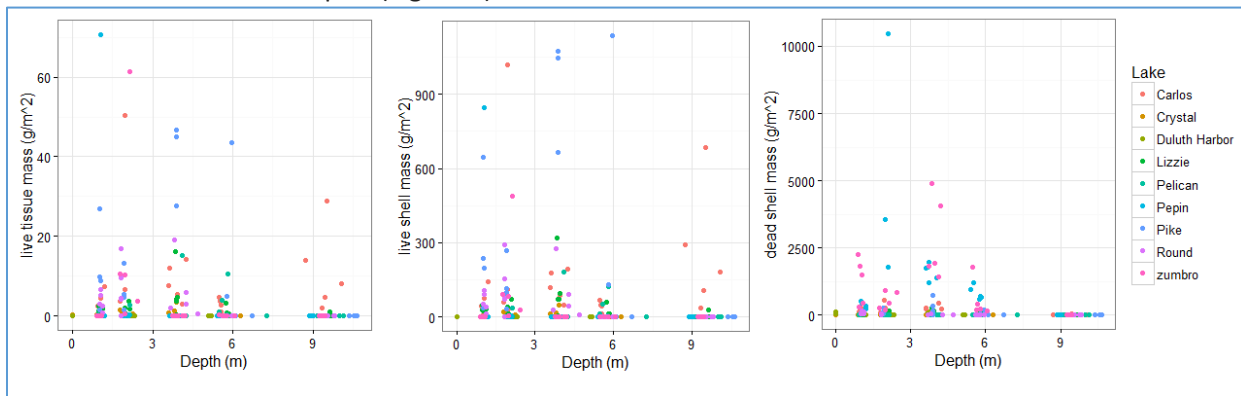


Figure 3: distribution of living tissue and shell and discarded shell material across depth in 9 MN lakes.

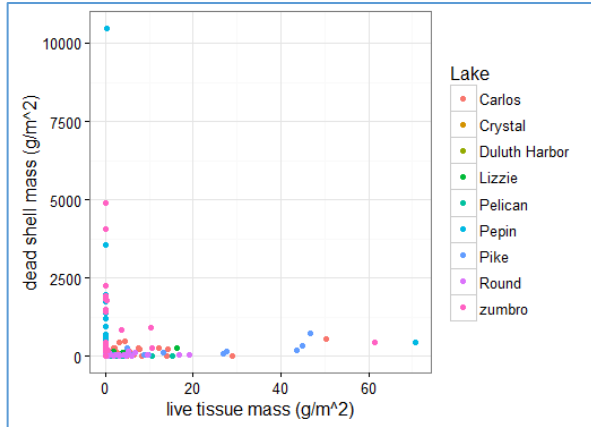


Figure 4: Relationship between live tissue and discarded shell biomass across study lakes.

### Tissue and shell composition

Dreissenid tissue and shell composition was generally variable between size classes and lakes (Figures 5,6; Table 1). Tissue P varied strongly between lakes but not as significantly between size classes, with no significant interaction between size and lake. Tissue C and N varied significantly between size classes and lakes with no significant interaction between size and lake. Soft tissue C and N composition was highest in large mussels. Shell P and N content varied significantly between mussel size classes and lakes, and tended to be highest in small mussels; there were significant size by lake interactions, suggesting inconsistent pattern of variation in N and P composition with size across lakes. Shell C composition was remarkably constant, not varying between sizes and lakes.

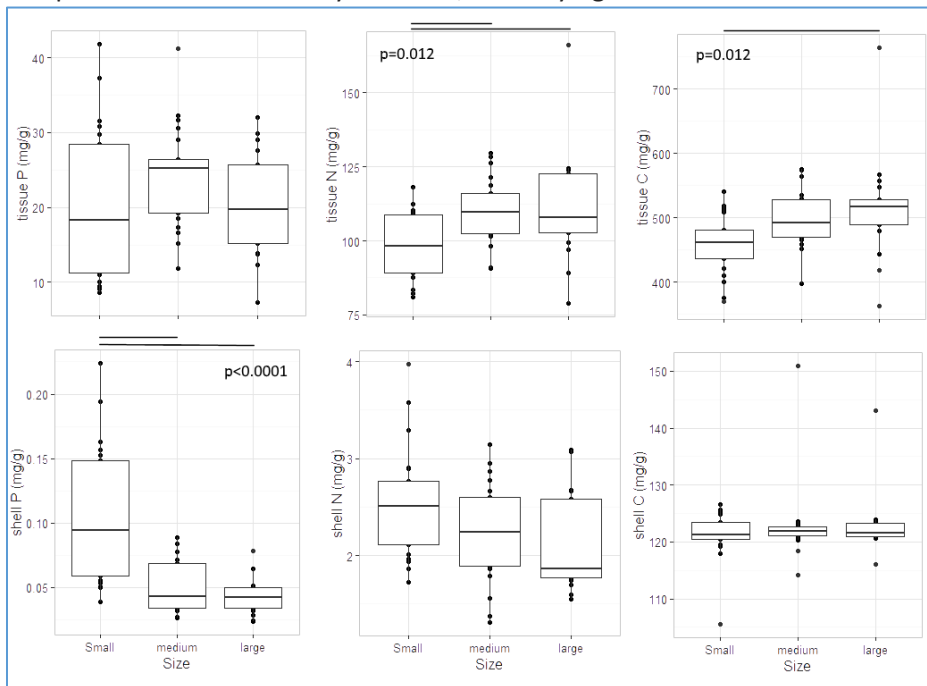


Figure 5: P, N and C composition in soft tissues and shells of dreissenids of different sizes across all lakes. P-values indicate significant inter-lake differences based on one-way ANOVA tests. Significant differences between size classes shown as black lines based on Tukey HSD post-hoc tests.

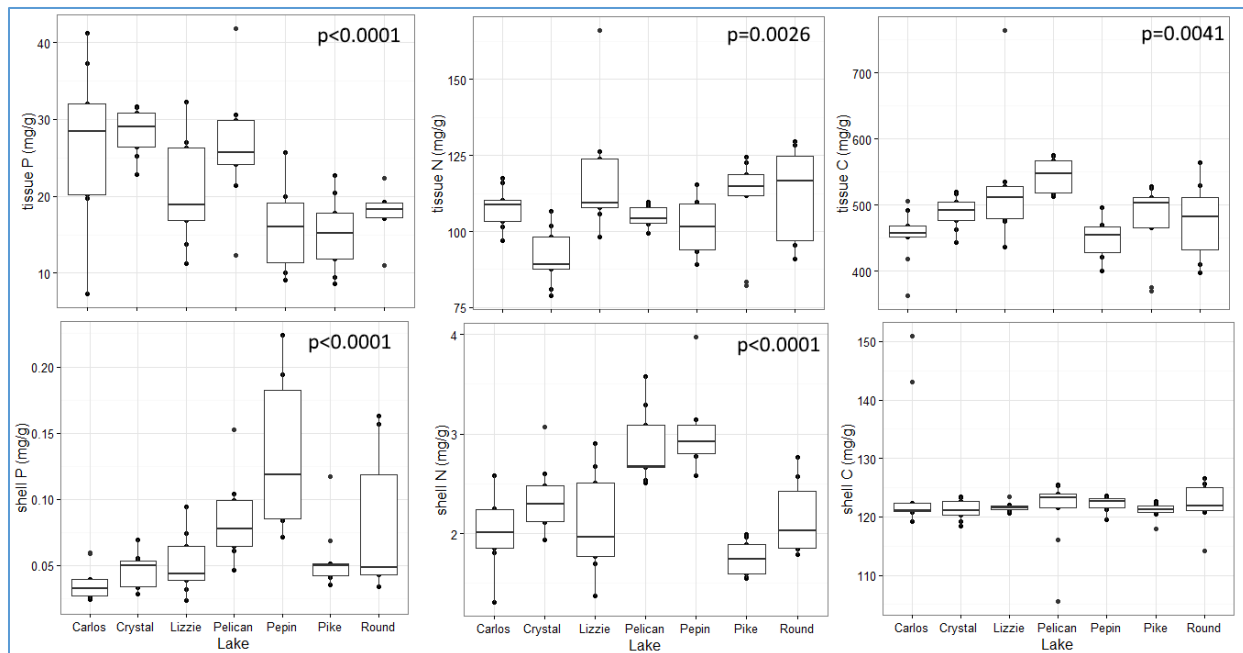


Figure 6: P, N and C composition in soft tissues and shells of dreissenids in different lakes across all mussel sizes. P-values indicate significant inter-lake differences based on one-way ANOVA tests.

Table 1: Results of two-way ANOVA tests on tissue and shell C, N and P composition.

| Parameter | Factor    | F-value | P-value |
|-----------|-----------|---------|---------|
| Tissue P  | Lake      | 6.72    | <0.0001 |
|           | Size      | 3.41    | 0.043   |
|           | Lake*Size | 1.24    | 0.29    |
| Tissue N  | Lake      | 5.08    | 0.0006  |
|           | Size      | 6.85    | 0.0028  |
|           | Lake*Size | 1.30    | 0.26    |
| Tissue C  | Lake      | 4.10    | 0.0028  |
|           | Size      | 5.06    | 0.011   |
|           | Lake*Size | 0.83    | 0.615   |
| Shell P   | Lake      | 23.36   | <0.0001 |
|           | Size      | 49.72   | <0.0001 |
|           | Lake*Size | 3.85    | 0.00085 |
| Shell N   | Lake      | 16.62   | <0.0001 |
|           | Size      | 5.42    | 0.0084  |
|           | Lake*Size | 2.10    | 0.044   |
| Shell C   | Lake      | 1.14    | 0.36    |
|           | Size      | 0.49    | 0.62    |
|           | Lake*Size | 0.70    | 0.73    |

### Lake wide biomass and C, N, P content

Combining mussel biomass estimates with tissue and shell elemental composition data allowed us to assess the total standing stocks of C, N and P contained in dreissenids in 7 lakes, as well as the distribution of P, N and C among different tissues of dreissenids (Table 2; Figure 7). In most lakes, the majority of P in dreissenids was in soft tissues, while about half of the N was in soft tissues and the other half distributed between live and discarded shell material. Most carbon associated with dreissenids was contained in live and discarded shell material. Standing stocks of P in the water column of 3 lakes were calculated based on total P measurements in water samples and lake volume; P stocks were calculated for only 3 lakes since total lake volume was not easily available for all lakes. In two lakes (Pepin, Carlos),

dreissenid tissues contained ~30% of standing P stocks in water. In another lake (Pike) dreissenids held more than 130% of the P in the water column. These results suggest that dreissenids can represent a significant pool for nutrients in some systems.

Table 2: Total biomass and C, N and P contained in dreissenids in 7 study lakes.

| Lake    | Area (acres) | soft tissue mass (tons) | live shell mass (tons) | dead shell mass (tons) | mussel C (tons) | Mussen N (tons) | Mussel P (tons) |
|---------|--------------|-------------------------|------------------------|------------------------|-----------------|-----------------|-----------------|
| Carlos  | 2605.11      | 5.0                     | 105.7                  | 322.7                  | 168.31          | 5.48            | 2.34            |
| Crystal | 1412.31      | 0.70                    | 9.6                    | 1.17                   | 4.95            | 0.26            | 0.06            |
| Lizzie  | 4035         | 3.62                    | 71.39                  | 105.1                  | 70.04           | 2.40            | 0.26            |
| Pelican | 271.38       | 7.64                    | 92.7                   | 2.38                   | 46.97           | 3.22            | 0.63            |
| Pepin   | 12299.5      | 159.55                  | 1476.3                 | 21730.8                | 5812.45         | 174.17          | 11.42           |
| Pike    | 488.27       | 5.28                    | 127.4                  | 46.99                  | 70.92           | 2.66            | 0.27            |
| Round   | 20           | 6.02                    | 97.99                  | 68.3                   | 69.46           | 3.02            | 0.37            |

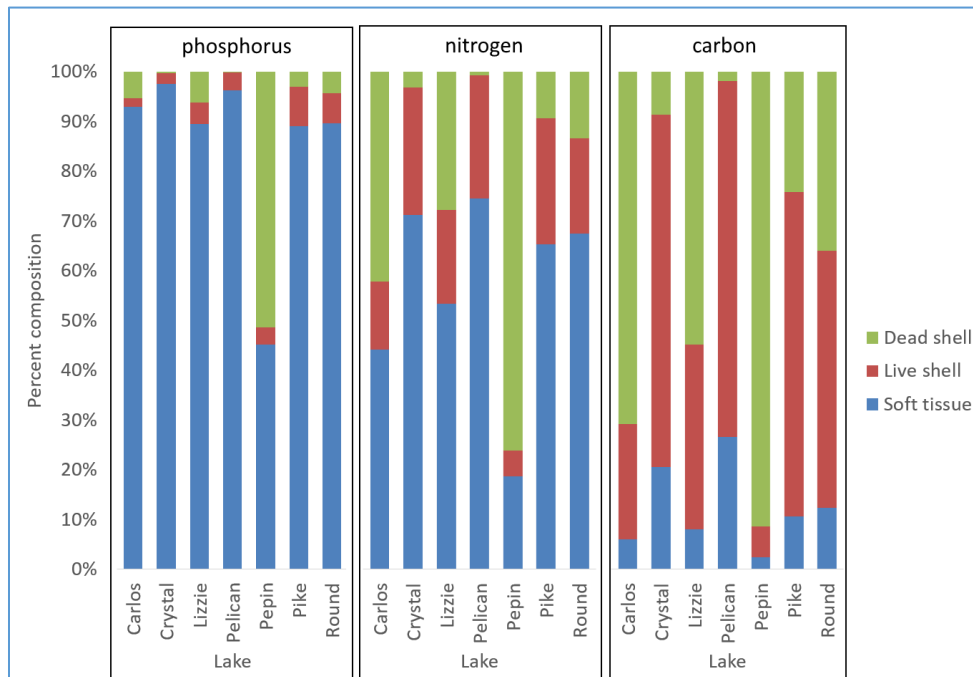


Figure 7: Distribution of P, N and C contained in dreissenid mussels among different compartments in different lakes.

**Next steps:**

The goal of constructing detailed nutrient budgets for dreissenids requires additional measurements to be made. In summer of 2016 we will return to the study lakes to retrieve shell dissolution experiments and perform measurements of dissolved and solid nutrient release rates by dreissenids. Shell dissolution experiments will help determine the long-term fate of dreissenid shell material and thus the C, N and P contained in discarded shell material. Measurements of nutrient excretion and deposition will be combined with tissue and shell nutrient concentration measurements to assess how dreissenids affect nutrients in different lakes and examine the factors that affect the extent to which dreissenid

establishment can shape nutrient dynamics. Future work will be performed by the MS student supported by this grant and funded from PI Ozersky's University of Minnesota start-up funds.

2) Publications:

None so far: project has been going on for one year and data collection and analyses are still in progress.

3) Student Support:

1 MS student was supported by this grant through Water Resource Sciences program at University of Minnesota Duluth; WRC funds covered 0.25 RA for one term (Sept.-Dec. 2015), which was supplemented from PI Ozersky's start-up funds and TAs from the biology department.

4) Presentations:

None so far: project has been going on for one year and data collection and analyses are still in progress. Presentation of results by MS student on project is scheduled at an international conference (Association for the Sciences of Limnology and Oceanography) in Santa Fe, NM, June 5-10 2016.

5) Awards:

None

6) Related Funding:

None

# Improving the (Bio)fouling and Mechanical Resistance of Ultrafiltration Membranes for Drinking Water Production

## Basic Information

|                                 |   |
|---------------------------------|---|
| <b>Title:</b>                   | Improving the (Bio)fouling and Mechanical Resistance of Ultrafiltration Membranes for Drinking Water Production |
| <b>Project Number:</b>          | 2015MN362B  |
| <b>Start Date:</b>              | 3/1/2015  |
| <b>End Date:</b>                | 2/28/2016   |
| <b>Funding Source:</b>          | 104B  |
| <b>Congressional District:</b>  | Minnesota fifth   |
| <b>Research Category:</b>       | Engineering   |
| <b>Focus Category:</b>          | Treatment, Water Quality, Water Use   |
| <b>Descriptors:</b>             | None  |
| <b>Principal Investigators:</b> | Santiago Romero Vargas Castrillón   |

## Publication

1. “Quantifying bacterial adhesion to polymeric membranes by single-cell force spectroscopy”. Sara BinAhmed, Anissa Hasane, and Santiago Romero-Vargas Castrillón. Poster to be presented at the Gordon Conference on Membrane Materials and Processes. July 31 – August 5, 2016, New London, NH

# 2015MN362B: Improving the (Bio)fouling and Mechanical Resistance of Ultrafiltration Membranes for Drinking Water Production

Nathan G. Karp and Santiago Romero-Vargas Castrillon (PI)

Department of Civil, Environmental, and Geo- Engineering

University of Minnesota, Minneapolis, MN 55455

## 1) Research Synopsis

### Problem Statement

Water scarcity is becoming an ever more prevalent problem worldwide due to climate change, population growth and urbanization, and over-exploitation of water resources.<sup>1, 2</sup> Technologies are needed that can improve the efficiency of water treatment processes and lend to greater water availability across the globe. Membrane-technologies are poised play a critical role in addressing this challenge due to their high spatial and removal efficiencies and their ability to operate without chemical additives. Such technologies are currently employed in the processes of microfiltration (MF), ultrafiltration (UF), nanofiltration (NF), and reverse osmosis (RO). Of these, MF and UF processes are most widely applied in drinking water plants, including the plant at Columbia Heights, MN, which provides the city of Minneapolis 78 million gallons of drinking water per day.<sup>3</sup>

Despite their advantages, all membrane processes are hindered by fouling, which is defined by IUPAC as “a process resulting in loss of performance of a membrane due to the deposition of suspended or dissolved substances on its external surfaces, at its pore openings or within pores.”<sup>4</sup> Given that UF processes require 3 kWh per m<sup>3</sup> of product water under normal operating conditions, the energy cost becomes increasingly prohibitive if membranes are fouled.<sup>5</sup> In the presence of fouling, pumping needs to be increased to achieve a higher transmembrane pressure in order to maintain flux. Additional costs are accrued when membranes need to be cleaned or replaced.<sup>6</sup> Furthermore, fouling of membranes decreases permeate water quality.<sup>7</sup> Thus, there is much to be gained from addressing the issue of membrane fouling, including cheaper and more efficient water treatment systems and reduced energy usage.

### Introduction

Two of the primary types of fouling are organic fouling due to the adsorption of natural organic matter (NOM) and biofouling due to the formation of a bacterial biofilm on the membrane surface.<sup>8</sup> Biofouling of membranes often occurs when an organic conditioning film is already present. Thus, targeting the formation of the organic fouling layer is effective in preventing subsequent fouling.

Organic fouling occurs most prevalently on surfaces that are hydrophobic, rough, and charged. Consequently, membrane surface modifications that yield a hydrophilic, smooth, and uncharged surface offer promising solutions capable of treating fouling.

Graphene and its derivatives have been widely utilized nanomaterials in recent years due to their smoothness, single-layer thickness, and potentially high water permeability.<sup>9, 10</sup> Graphene oxide (GO) can be easily produced through chemical exfoliation of graphite, yielding a 2D sheet structure containing polar carboxylic acid, epoxide, and hydroxyl groups.<sup>11</sup> In addition to its hydrophilicity, GO has been shown to inactivate both Gram-positive and Gram-negative bacteria.<sup>11-14</sup> Thus, GO has great potential to be used in membrane technologies to mitigate both organic and biofouling.

The current research aims to impart antifouling properties to the surface of polysulfone (PSf) UF membranes through a GO surface-coating layer. Several previous studies had attempted to achieve these results by incorporating GO into the polymer dope solution used to form the membrane material, but the surface interactions were minimized as the material was embedded in the polymer matrix and not concentrated on the membrane surface.<sup>15-18</sup> Only two studies had used post-fabrication surface modification of a membrane with GO: the work of Perreault et al.<sup>14</sup>, in which amine coupling was used to covalently attach graphene oxide to forward osmosis membranes; and the recent work by Hegab et al.<sup>22</sup>, which reported the use of polydopamine (PDA) to immobilize GO on the surface of forward osmosis membranes. Our research has focused on the use of PDA to adhere GO to the surfaces of UF membranes. PDA is able to effectively coat most surfaces and has been incorporated with GO (hereafter referred to as PDA-GO) to coat surfaces.<sup>19, 20</sup> Through hydrogen bonding and  $\pi$ - $\pi$  interactions, PDA is believed to facilitate the adhesion of GO to the membrane and yield a uniform antifouling layer.

## **Methods and Materials**

### *Synthesis and Characterization of GO*

Graphene oxide (GO) was prepared via chemical exfoliation of graphite (Bay Carbon, SP-1, 325 mesh) using a modified Hummers method.<sup>23</sup> First, 2.0 g of graphite was placed in 5 mL of concentrated sulfuric acid at 80°C. Next, 2.0 g each of  $K_2S_2O_8$  and  $P_2O_5$  were added and the suspension was allowed to react at 80°C for 4.5 hours. After reaction, the mixture was transferred into 320 mL of ultrapure water and allowed to rest overnight. The mixture was subsequently vacuum filtered using PTFE membranes (0.45  $\mu$ m, Whatman TE 36) and dried overnight at room temperature. Next, the obtained black solid was placed into 80 mL of concentrated sulfuric acid over an ice bath, and 10.0 g of  $KMnO_4$  was slowly added so that the temperature of the mixture did not exceed 10°C. The mixture was then slowly heated to 35°C over a period of 2.5 hours. Next, 154 mL of ultrapure water was slowly added, not allowing the suspension to exceed 50°C, and reacted for 2 hours at room temperature. Lastly, the mixture was transferred to 480 mL of ultrapure water, and 8.4 mL of 30%  $H_2O_2$  was added, causing the mixture to acquire a yellowish-brown color. The suspension was allowed to rest for 2 days, and the precipitate was subsequently recovered by several steps of centrifugation (12,000 x *g*, 30 min), initially re-suspending the product in 10% HCl to remove chemical residues and finishing with resuspension in water until the

supernatant reached a pH of about 3.5. Finally, the suspended product was purified via dialysis (3.5 kDa membranes, Spectrum Labs) for 4 days and freeze dried via lyophilization for 4 days.

Raman spectroscopy (Witec Alpha300R) was used to confirm the oxidized graphitic structure. Atomic force microscopy (AFM) was used to determine the size and thickness of the GO sheets.

### *Fabrication and Characterization of Ultrafiltration Membranes*

Polysulfone ultrafiltration membranes were prepared as described by Zodrow et al.<sup>24</sup> First, 10.0 g of poly(vinylpyrrolidone) (PVP, MW: 58,000, Acros Organics) was dissolved in N-methyl-2-pyrrolidone (NMP, 99.5%, Sigma-Aldrich) by stirring with heat for 2 hours. Next, 15.0 g of polysulfone (PSf, MW: 22,000, Sigma-Aldrich) was added to the mixture and dissolved by stirring with heat for an additional 6 hours. The polymer dope solution was then stored in a desiccator overnight to remove any air bubbles.

Glass plates were wrapped in polyethylene terephthalate (PET) fabric and wrinkles were removed from the surface. The surface was then wetted with NMP and gently wiped with a tissue to remove excess solvent. Dope solution (~10-15 mL) was poured on the top of the glass plate and spread over the fabric using a casting blade set to a height of 250  $\mu\text{m}$ . The plate was then cast into a water nonsolvent bath, inducing phase inversion and precipitation of the polymer. After 10 minutes, the plate was removed from the bath and transferred to a secondary water bath for 1 hour. The membrane was then cut from the plate and refrigerated in ultrapure water until use.

The cross-section morphology of the membranes was observed using scanning electron microscopy (SEM, JEOL 6700). Prior to conducting SEM, membranes were freeze-fractured after removal of water and immersion in liquid nitrogen and sputter coated with 50  $\text{\AA}$  Pt. The permeability of the membranes was determined by mounting a 25 mm circular sample into an Amicon 8010 Stirred Cell. Pure water flux (PWF) was measured by weighing the permeate water after 10 second intervals at pressures of 10, 20, 30, 40, and 50 PSI.

### *Surface Functionalization of Membranes*

Polydopamine (PDA) was prepared in varying concentrations, under two different oxidizing conditions, and with or without direct incorporation with GO. Tris buffer (10mM) was prepared by diluting Trizma hydrochloride solution (Sigma) in water and adding NaOH until a pH of 8.5 was reached. Dopamine hydrochloride (Sigma) was dissolved in the solution at 4 g/L, turning it a light brown color. A modified procedure for preparing PDA coatings under strongly oxidizing conditions was also employed. This method, described by Zhang et al.<sup>21</sup>, involves dissolving 2 g/L dopamine HCl in 50 mM Tris buffer containing 5 mM  $\text{CuSO}_4$  and 19.6 mM  $\text{H}_2\text{O}_2$ .<sup>21</sup> In some experiments, GO was incorporated into the PDA solution. After dissolving dopamine HCl, GO dispersion (stabilized by sonication) was added to the mixture and stirred 2 minutes.

To functionalize the surface of membrane samples, square polypropylene frames were used to hold the sample in place and contain the coating solution, exposing only the surface of the membrane to the modification. Coating solution was poured into the frame, and the process was carried out with agitation using a benchtop shaker. In most experiments, PDA functionalization was followed by a rinsing step and subsequent GO functionalization. In some experiments, only a single functionalization (either PDA or GO-incorporated PDA) was used. Table 1 details the experimental conditions used.

### Characterization of Surface-Functionalized Membranes

Raman spectroscopy was used to determine the presence of GO on the membrane surface. Water contact angle measurements (Kyowa MCA-3) were performed to assess the hydrophobicity of modified membranes. The water permeability of the coated membranes was determined using a stirred cell.

**Table 1:** Methodologies of coating UF membrane with PDA-GO. The upper portion of the table describes the first, base PDA or PDA-GO coating layer, indicating the concentration of Tris buffer and PDA, concentration of GO incorporated, oxidation conditions, number of depositions, time for each deposition, and shaking velocity. The lower portion of the table describes the second coating layer, if any, consisting of concentration of GO and the number, time, and speed of depositions. As an example of reading the table, Sample #6 was subjected first to a 2 g/L CuSO<sub>4</sub>/H<sub>2</sub>O<sub>2</sub>-oxidized PDA solution in 50 mM Tris buffer for one deposition at 75 rpm for 40 minutes. It was subsequently coated three times for 15 minutes each at 75 rpm with 100 mg/L GO, and once for 60 minutes at 0 rpm with 100 mg/L GO.

| First Coat  |                 |                |                |                   |         |                |          |
|-------------|-----------------|----------------|----------------|-------------------|---------|----------------|----------|
| Samp#       | Tris Conc. (mM) | PDA Conc (g/L) | GO Inc. (mg/L) | Oxidation         | # Deps. | Dep. Time(min) | Dep. rpm |
| 1           | 10              | 4              | -              | Air               | 3, 1    | 15, 60         | 75, 0    |
| 2           | 50              | 2              | -              | CuSO <sub>4</sub> | 1       | 40             | 75       |
| 3           | 50              | 2              | 80             | CuSO <sub>4</sub> | 1       | 40             | 75       |
| 4           | 50              | 2              | 200            | CuSO <sub>4</sub> | 1       | 40             | 75       |
| 5           | 50              | 2              | 500            | CuSO <sub>4</sub> | 1       | 40             | 75       |
| 6           | 50              | 2              | -              | CuSO <sub>4</sub> | 1       | 40             | 75       |
| 7           | 50              | 2              | -              | CuSO <sub>4</sub> | 1       | 40             | 75       |
| 8           | 50              | 2              | 200            | CuSO <sub>4</sub> | 1       | 40             | 75       |
| 9           | 50              | 2              | 200            | CuSO <sub>4</sub> | 1       | 40             | 75       |
| 10          | 50              | 2              | 200            | CuSO <sub>4</sub> | 1       | 40             | 75       |
| 11          | 50              | 2              | -              | Air               | 1       | 40             | 75       |
| 12          | 50              | 2              | -              | CuSO <sub>4</sub> | 1       | 40             | 75       |
| Second Coat |                 |                |                |                   |         |                |          |
| Samp#       | Solution        | Conc. (mg/L)   |                |                   | # Deps. | Dep. Time(min) | Dep. rpm |
| 1           | GO              | 1000           |                |                   | 3, 1    | 15, 60         | 75, 0    |
| 2           | GO              | 1000           |                |                   | 3, 1    | 15, 60         | 75, 0    |
| 3           | -               | -              |                |                   | -       | -              | -        |
| 4           | -               | -              |                |                   | -       | -              | -        |
| 5           | -               | -              |                |                   | -       | -              | -        |
| 6           | GO              | 100            |                |                   | 3, 1    | 15, 60         | 75, 0    |
| 7           | GO              | 300            |                |                   | 3, 1    | 15, 60         | 75, 0    |
| 8           | GO              | 100            |                |                   | 3, 1    | 15, 60         | 75, 0    |
| 9           | GO              | 300            |                |                   | 3, 1    | 15, 60         | 75, 0    |
| 10          | GO              | 1000           |                |                   | 3, 1    | 15, 60         | 75, 0    |
| 11          | GO              | 1000           |                |                   | 3, 1    | 15, 60         | 75, 0    |
| 12          | GO              | 1000           |                |                   | 3, 1    | 15, 60         | 75, 0    |

### *Exposure of Surface-Functionalized Membranes to Stress Conditions*

To determine the robustness of the PDA-GO coating layers, various physical and chemical stress conditions were applied to modified membranes. Raman spectroscopy was used to assess any loss of GO on the surface, and contact angle measurements yielded the effects on surface hydrophobicity. Stress conditions utilized included sonication for 10 minutes in DI water, saturated (1.17 g/mL) KCl, or 1M NaOH, exposure for 72 hours to saturated KCl or NaOH, rinsing with water from a squirt bottle, and physical contact with the surface via gentle wiping motion.

## **Results and Discussion**

### *Characterization of GO Using Raman Spectroscopy and AFM*

Raman spectroscopy (Figure 1) confirmed the successful synthesis of GO, exhibiting the characteristic D and G bands at  $\sim 1350\text{ cm}^{-1}$  and  $1590\text{ cm}^{-1}$  respectively.

AFM was used in tapping mode to determine the relative size and thickness of GO nanosheets deposited on an ultraflat silicon wafer. As indicated in Figure 2, the sheets were found to be on the order of hundreds of nanometers wide and 1.3 nm thick.

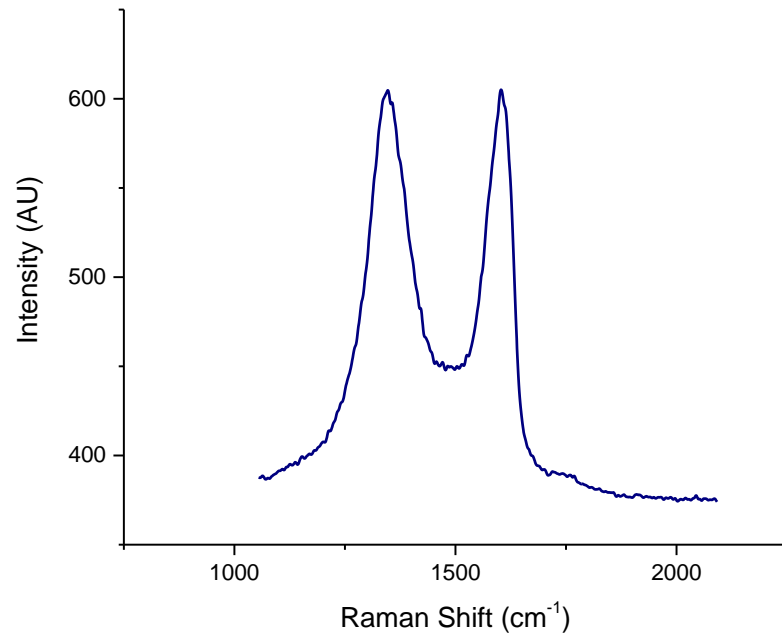


**Figure 1:** Raman spectrum exhibiting the D and G bands indicative of graphene oxide. The GO suspension was deposited on a silicon wafer before measurement of the Raman spectrum.

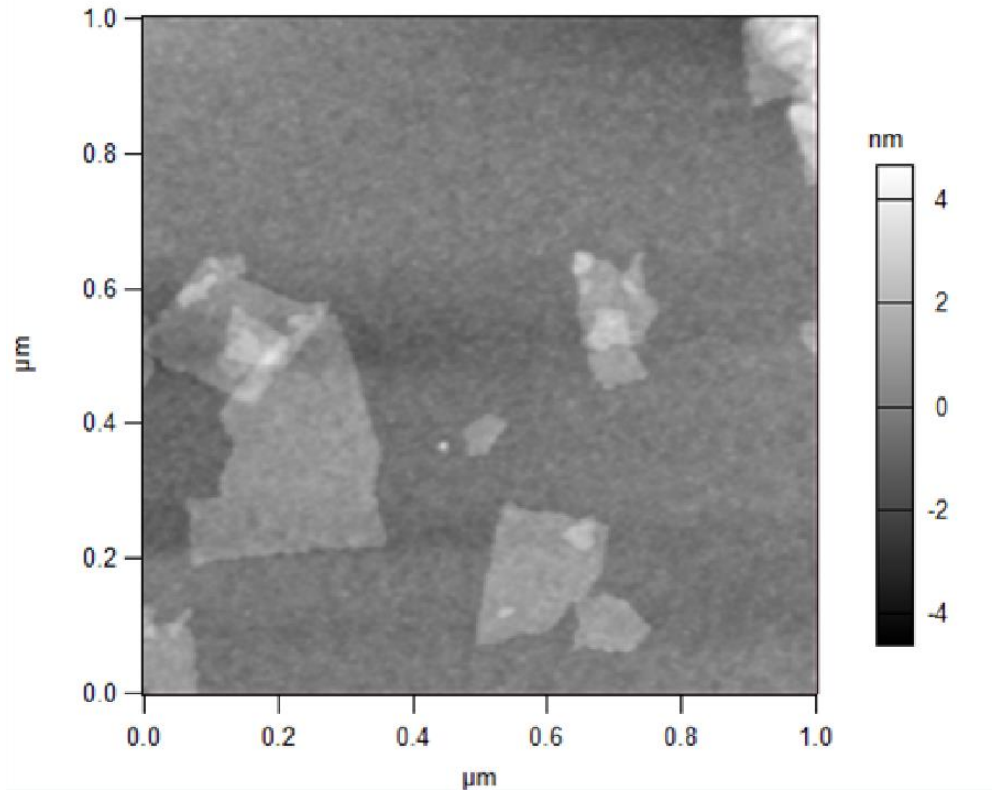


**Figure 2:** AFM image of graphene oxide nanosheets deposited on a silicon wafer. The sheets were found to be a  $\sim 100$  nm in width and  $\sim 1.3$  nm thick.

#### *Cross-Sectional SEM of UF Membranes Reveals Pillar Structure*

Cross-sectional imaging of Pt coated, freeze-fractured UF membranes using SEM (Figure 3) revealed a pillar-like morphology similar to that observed by Zodrow et al.<sup>24</sup>

#### *Coating Procedures Successfully Functionalize Membranes with GO and Increase Surface Hydrophilicity*

After initial coating using the Sample #1 composition detailed in Table 1 (air oxidation, no incorporation of GO into the PDA solution), Raman spectroscopy (Figure 4) confirmed the success of the coating procedure, as indicated by the presence of the D and G bands. Subsequent contact angle measurements (Figure 5) on pristine, PDA coated, and PDA-GO coated samples revealed that the GO coating yielded membrane surfaces that were much more hydrophilic ( $40.7 \pm 5.7^\circ$ ) than either pristine ( $65.2 \pm 3.5^\circ$ ) or PDA-coated ( $57.6 \pm 3^\circ$ ) samples.

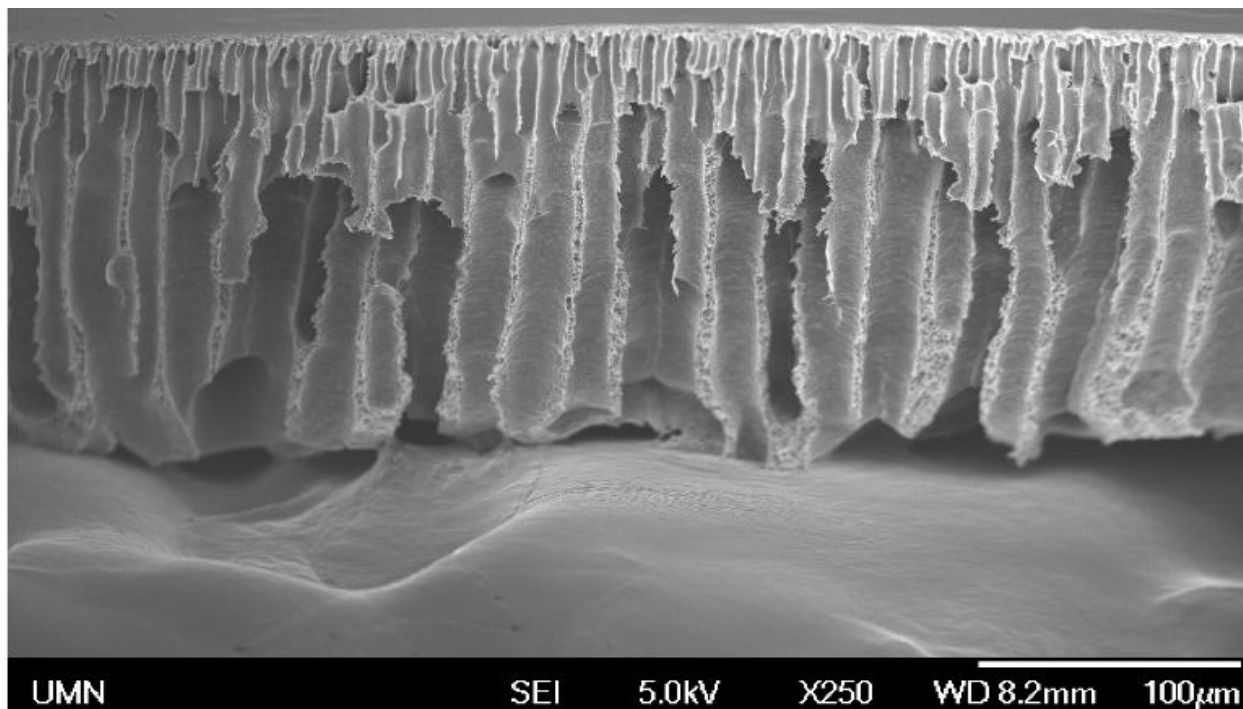


**Figure 3:** SEM micrograph showing the cross-section morphology of the fabricated UF membranes.

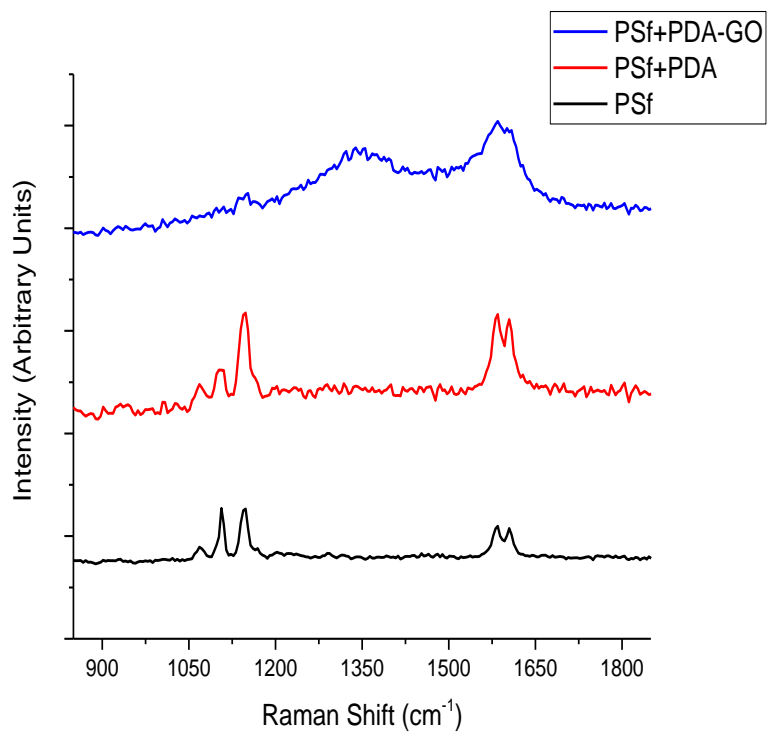


**Figure 4:** Raman spectrum comparing pristine, PDA coated, and PDA-GO coated membrane samples. The Sample #1 composition as indicated in Table 1 was used. Note the presence of the D and G bands of GO.

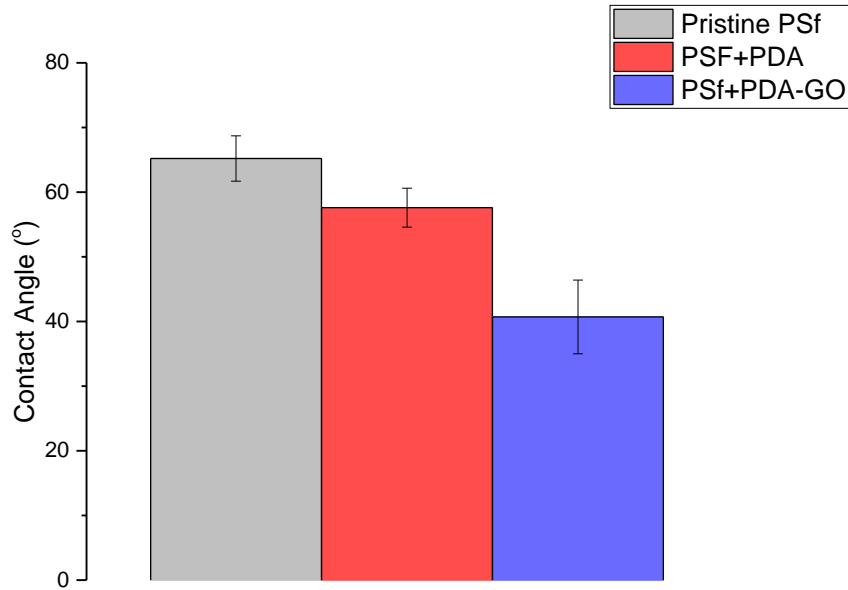


**Figure 5:** Contact angle measurements comparing pristine, PDA-coated, and PDA-GO coated membrane samples. The Sample #1 composition as indicated in Table 1 was used. Coating with PDA-GO was observed to significantly decrease the contact angle compared to pristine and PDA coated samples. The right- and left-hand side contact angles of 10 randomly placed droplets of water were measured, and three separately fabricated and coated samples were used for each sample type.

*Resistance Towards Basic Conditions is Improved with  $\text{CuSO}_4/\text{H}_2\text{O}_2$ -Oxidized PDA-GO Coatings Compared to Air-Oxidized Ones*

To assess the robustness of the PDA-GO coating layer, membranes coated using the Sample #1 composition were exposed to stress conditions, including sonication for 10 minutes in 1M NaOH or saturated KCl and exposure for 72 hours to 1M NaOH or saturated KCl. Figure 6 depicts Raman spectra for each of these conditions compared to the pristine and unstressed samples. It was observed that, while resistant to the high electrolyte concentration conditions, the PDA-GO coating layer was significantly affected by the strong base, as indicated by the diminished D and G bands (higher  $I_{1147}/I_{1585}$  ratio).

To address this issue, a modification to the coating procedure based on Zhang et al. was used, as described by the Sample #2 composition in Table 1.<sup>21</sup> The modification utilized stronger oxidizing conditions (a mixture of  $\text{CuSO}_4$  and  $\text{H}_2\text{O}_2$ ) to increase the polymerization rate of PDA. This method is reported to exhibit increased resistance towards various chemical stressors, including  $\text{NaOH}$ <sup>21</sup>. After exposure of these membranes to the same set of stress conditions as Sample #1, Raman spectroscopy (Figure 7) revealed resistance towards NaOH. Thus, each subsequent membrane sample utilized these new oxidizing conditions to impart better coating layer robustness.

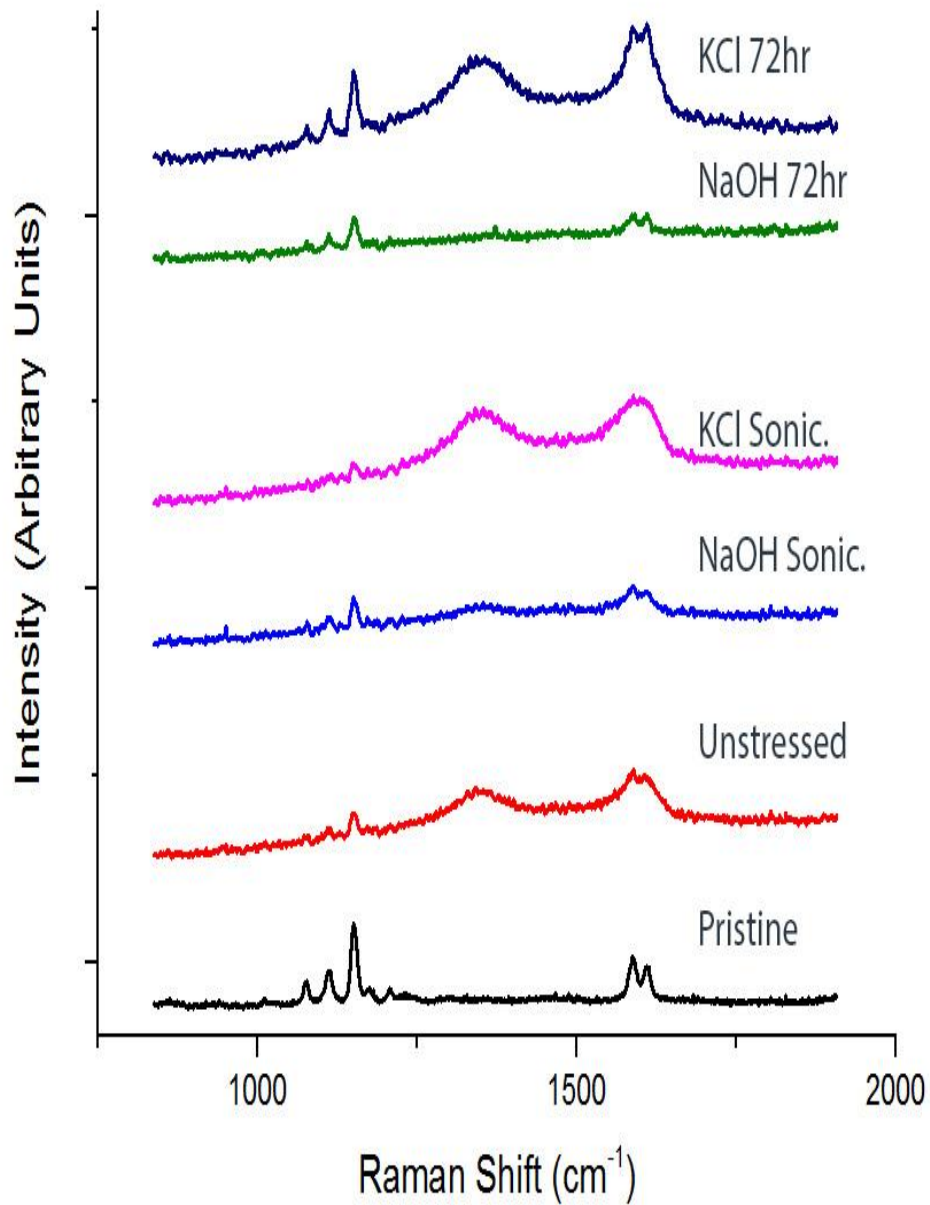


**Figure 6:** Raman spectra comparing stressed coated membrane samples to pristine and unstressed samples (Sample #1). The PDA-GO layer was observed to remain intact after exposure to and sonication in saturated KCl for 72 hours and 10 minutes respectively. Similar exposure to 1M NaOH however, removed most of the GO, as indicated by the diminished D and G bands (higher  $I_{1147}/I_{1585}$  ratio).

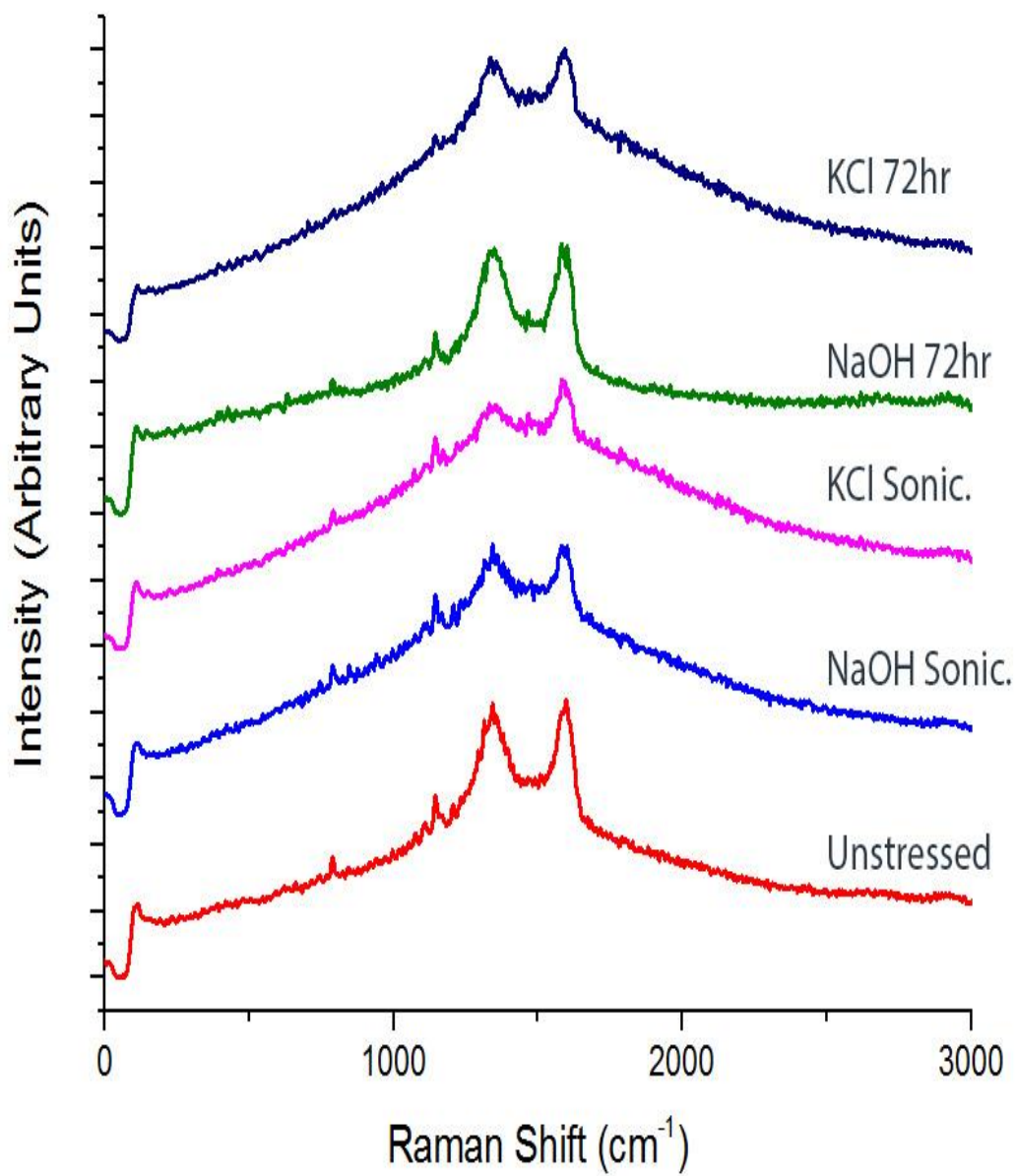


**Figure 7:** Raman spectra comparing stressed coated membrane samples to pristine and unstressed samples (Sample #2 in Table 1). Utilizing stronger oxidation conditions was found to impart robustness of the PDA-GO coating layer towards basic conditions.

### *PDA-GO Coatings Are Removed by Mechanical Shearing*

It was discovered that, upon physical contact with PDA-GO coated membranes, the coating layer could be removed, as if it were a loosely attached layer on the surface. To assess the extent that this removed the coating layer, and to expose it to additional physical stress, membrane samples coated using the Sample #2 composition were rinsed for 10 seconds with water from a squirt bottle and gently sheared with a gloved finger. Raman spectroscopy (Figure 8) was conducted and it was observed that nearly all of the GO had been removed from physical contact. The force of the DI water stream from rinsing, however, was not enough to significantly remove the GO layer.

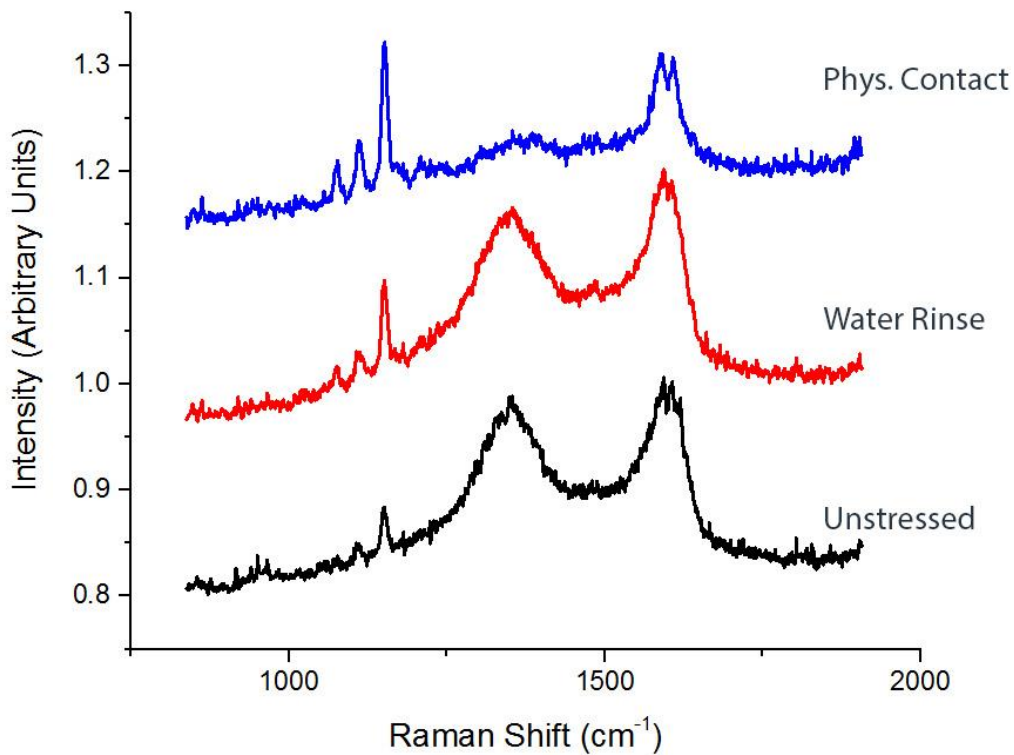


**Figure 8:** Raman spectra comparing membranes coated using the Sample #2 composition after exposure to a rinsing water stream and physical contact (wiping) to an unstressed sample. The D and G bands are significantly diminished after exposure to physical contact, but not rinsing.

### *Drying Coated Membrane Samples does not Improve Resistance to Mechanical Shearing*

In an attempt to strengthen the PDA-GO coating layer and avoid removal upon physical contact, Sample #2 membranes were dried at 30 °C overnight. After drying, the membranes were subjected to rinse and mechanical shear stresses. Raman spectroscopy (Figure 9) still showed removal of GO after contact. Additionally, the drying period was found to profoundly diminish the permeability of the

membrane samples as a result of pore collapse. An attempt was made to minimize this effect by drying for a shorter period of time, but the surface coating required an overnight drying period in order to dry completely.

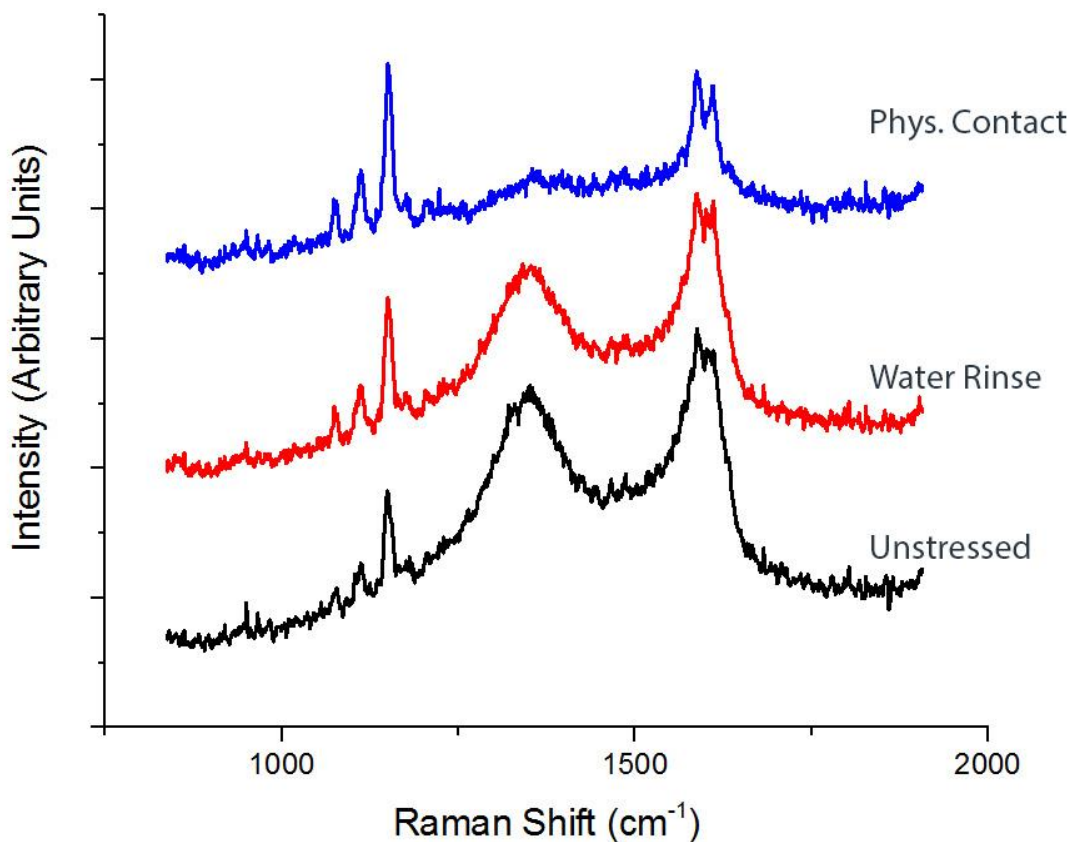


**Figure 9:** Raman spectra comparing membranes coated using the Sample #2 composition dried overnight after exposure to a rinsing water stream and physical shearing (wiping) to an unstressed sample. As with the undried sample, the D and G bands are significantly diminished after exposure to physical contact, but not rinsing.

#### *Incorporation of GO into PDA Coating Solution Yields Contact-Resistant Coatings but Less Hydrophilic Surfaces*

To address the lack of resistance towards physical contact, a modified coating procedure based on Hegab et al. was utilized (Samples 3-5 in Table 1).<sup>22</sup> The procedure involves the incorporation of GO into the PDA solution, requiring only a single deposition. Three different concentrations of GO were used (80 ppm, 200 ppm, and 500 ppm). Exposure to rinsing, physical contact, sonication in water, and sonication in NaOH revealed that membranes coated using this method were resistant to physical contact but not to basic conditions. Figure 10 indicates the Raman spectra for Sample #3 (80 ppm GO);

similar spectra were observed for Samples #4 and #5 (200 ppm GO and 500 ppm GO, respectively). Furthermore, contact angle measurements (Figure 11) on these samples revealed that they were much less hydrophilic than samples coated with separate layers of PDA and GO. This is consistent with the much less prominent D and G bands observed in the Raman spectra.

Combining the methods previously used by adding a base coating layer of GO-incorporated PDA and subsequently depositing GO on top recovered hydrophilicity but led, once again, to vulnerability towards strong basic conditions. This was observed for three different concentrations of the second GO coating layer (Samples 8-10 in Table 1).

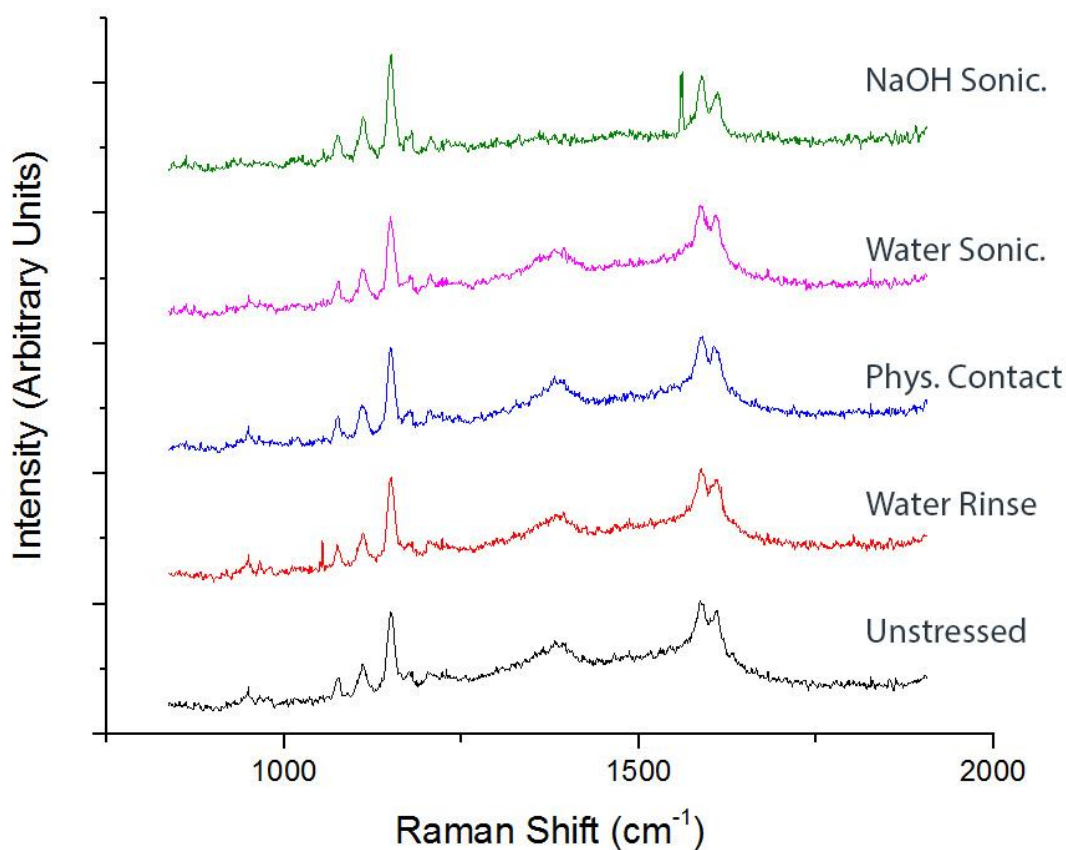


**Figure 10:** Raman spectra comparing stressed membrane samples to unstressed utilizing a GO-incorporated PDA solution. Sample #3 was resistant towards rinsing, sonication in water, and physical contact, but not towards sonication in NaOH. Similar results were observed for Samples #4 and #5, which incorporated different concentrations of GO.

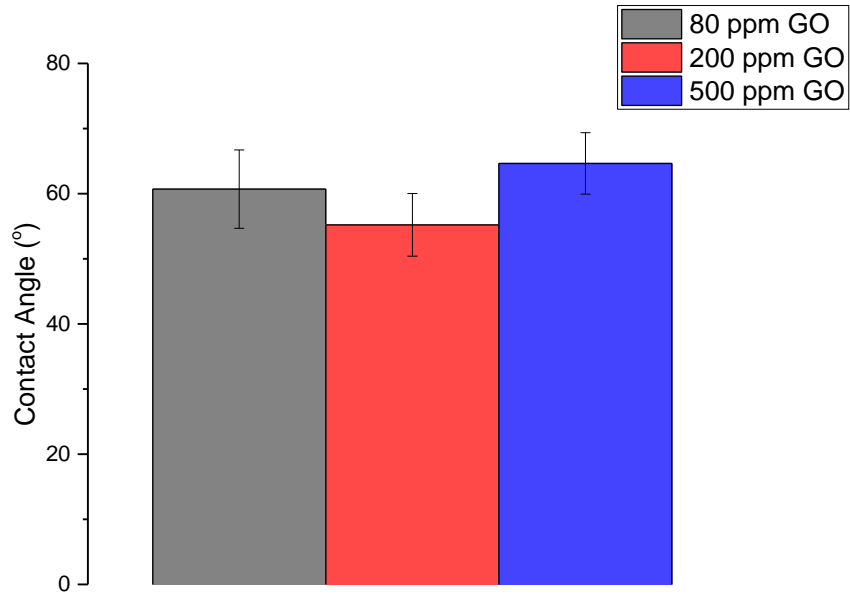


**Figure 11:** Contact angle measurements on Samples #3, 4, and 5. All samples were observed to be much more hydrophobic than samples coated with PDA and GO separately, and similar in hydrophobicity to pristine PSf membranes.

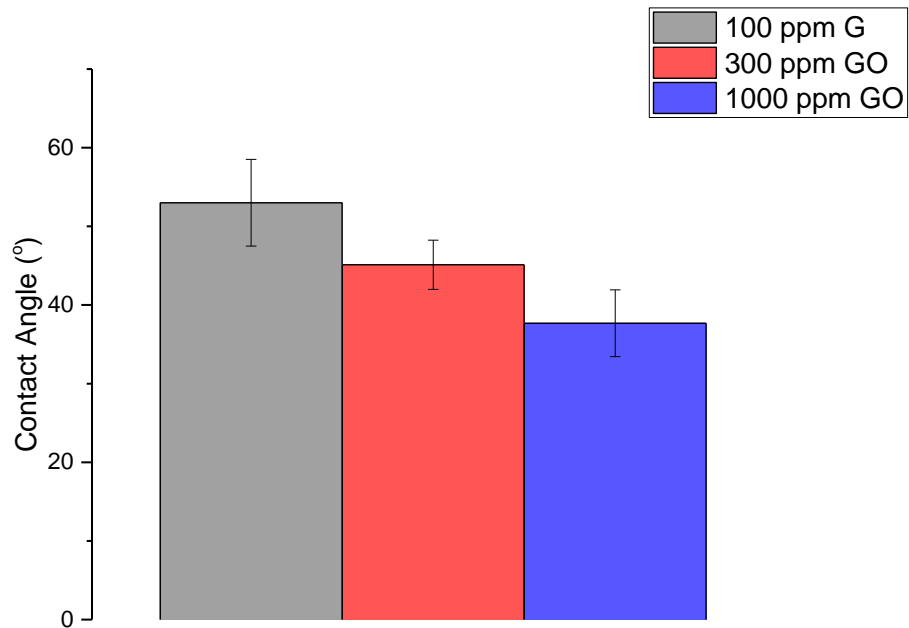


**Figure 12:** Contact angle measurements on membrane samples coated using three different concentrations of GO. Samples #6, #7, and #2 used 100 ppm, 300 ppm, and 1000 ppm respectively.

### *Surface Hydrophilicity Increases with Increasing GO Concentration*

A modification to the coating procedure used for Sample #2 was made by using a lower GO concentration (Samples #6 and #7). Raman spectroscopy revealed that, as in Sample #2, the coating layer was resistant towards basic conditions but not to physical contact. Contact angle measurements (Figure 12) revealed that using a lower concentration of GO results in more hydrophobic interfaces.

### *PDA and PDA-GO Surface Modifications do not Negatively Affect Membrane Permeability*

Samples #11 and #12 sought to make a more reliable comparison between coating methods using air-oxidized and CuSO<sub>4</sub>/H<sub>2</sub>O<sub>2</sub>-oxidized PDA solutions. Stress tests and Raman spectroscopy revealed similar results as before, with the stronger oxidizing conditions imparting greater resistance towards basic conditions.

The permeability of these membranes was measured and compared with pristine samples from the same original membrane. For both Sample #11 and Sample #12, a single PDA coated and a single PDA-GO coated sample were characterized and compared to three pristine samples. Results (Table 2) indicated that these coating layers do not negatively affect membrane permeability, and may even increase permeability, although further replicates would be needed to assess the statistical significance of this observation.

**Table 2:** Comparison of permeabilities of pristine, PDA coated, and PDA-GO coated membranes coated using both air and enhanced PDA oxidation. Coating layers are observed not to negatively affect permeability in both samples and may increase permeability, although further replications are needed.

| Permeability (LMH/Bar) |                   |            |     |        |
|------------------------|-------------------|------------|-----|--------|
| Samp#                  | Oxidization       | Pristine   | PDA | PDA-GO |
| 11                     | Air               | 274 ± 24.5 | 313 | 366    |
| 12                     | CuSO <sub>4</sub> | 284 ± 20.0 | 327 | 430    |

### **Conclusions**

PDA-GO coatings have been shown to be a promising surface modification for UF membranes, as they greatly increase hydrophilicity without affecting the membrane's permeability. Formulation of GO coating that exhibits resistance towards highly basic conditions and physical contact remains a challenge. It has been found that using separate coating processes for PDA and GO yields the most hydrophilic surface, whereas membranes coated with PDA incorporated with GO give little to no additional hydrophilicity. Using CuSO<sub>4</sub> and H<sub>2</sub>O<sub>2</sub> as oxidizing agents to assist in the polymerization of dopamine improves resistance towards basic conditions. However, these coatings remain susceptible to

removal by physical contact (mechanical shearing) unless PDA and GO are incorporated together. Drying, lowering the concentration of GO, and combining methods have been proven not to add any additional physical resistance. Table 3 summarizes the data.

**Table 3:** Summary of Raman intensity ratios for unstressed, NaOH sonicated, and physically contacted samples as well as water contact angles of unstressed samples. Hydrophilicity is assessed as high (green) if the contact angle is 45° or lower, low (red) if it is 53° or higher, and medium (yellow) if it is in between those values. Resistance towards stressors is determined by comparison of intensity ratios (I1147/I1585) to the unstressed sample. No resistance ("No") is assigned whenever the stressed sample exhibits an intensity ratio statistically similar to the uncoated sample. "Yes", denoting some resistance to NaOH or physical shearing stress, is assigned whenever the intensity ratio is statistically different from the uncoated sample.

| Samp#    | Unstressed    | Unstressed | NaOH Sonic    | Phys. Contact | Hydrophilic | Base Resistant | Contact Resistant |
|----------|---------------|------------|---------------|---------------|-------------|----------------|-------------------|
|          | I1147/I1585   | Cont. Ang. | I1147/I1585   | I1147/I1585   |             |                |                   |
| Pristine | 1.076 ± 0.012 | 65.2 ± 3.5 | -             | -             |             | -              | -                 |
| 1        | 0.897 ± 0.012 | 40.7 ± 5.7 | 0.962 ± 0.034 | -             |             | No             | -                 |
| 2        | 0.732 ± 0.053 | 37.7 ± 4.2 | 0.855 ± 0.086 | 0.977 ± 0.009 |             | Yes            | No                |
| 3        | 0.949 ± 0.016 | 60.7 ± 6.0 | 0.998 ± 0.005 | 0.956 ± 0.010 |             | No             | Yes               |
| 4        | 0.979 ± 0.008 | 55.2 ± 4.8 | 0.999 ± 0.007 | 0.980 ± 0.002 |             | No             | Yes               |
| 5        | 0.988 ± 0.013 | 64.6 ± 4.7 | 1.002 ± 0.002 | 0.989 ± 0.011 |             | No             | Yes               |
| 6        | 0.790 ± 0.011 | 53.0 ± 5.5 | 0.890 ± 0.051 | 0.952 ± 0.012 |             | Yes            | No                |
| 7        | 0.825 ± 0.039 | 45.1 ± 3.1 | 0.840 ± 0.075 | 0.955 ± 0.011 |             | Yes            | No                |
| 8        | 0.822 ± 0.036 | 47.9 ± 3.6 | 0.838 ± 0.013 | 0.984 ± 0.008 |             | Yes            | No                |
| 9        | 0.902 ± 0.034 | 50.9 ± 4.3 | 0.934 ± 0.016 | 0.963 ± 0.004 |             | Yes            | No                |
| 10       | 0.758 ± 0.027 | 50.2 ± 3.4 | 0.821 ± 0.107 | 0.988 ± 0.014 |             | Yes            | No                |
| 11       | 0.822 ± 0.068 | 37.3 ± 4.4 | 0.956 ± 0.019 | 0.978 ± 0.005 |             | No             | No                |
| 12       | 0.720 ± 0.044 | 30.5 ± 4.6 | 0.784 ± 0.021 | 0.937 ± 0.014 |             | Yes            | No                |

## Future Work

Preliminary tests indicate that PDA-GO may impart antibacterial activity to the membrane surface, and that PDA oxidized with CuSO<sub>4</sub> contributes greatly to this effect due to the presence of Cu ions. The effect of the GO coatings on membrane transport properties and rejection coefficient needs to be further evaluated. Membrane surface properties such as roughness, streaming potential and pore size distribution will also be evaluated. Lastly, the ability for the membrane to mitigate fouling will be evaluated using synthetic foulant solutions.

## Acknowledgements

This research was funded by the USGS National Competitive Grants Program. Parts of this work were carried out in the Characterization Facility, University of Minnesota, which receives partial support from NSF through the MRSEC program.

## References

1. Shannon, M.A., et al., *Science and technology for water purification in the coming decades*. Nature, **2008**. 452(7185): p. 301-310.
2. Elimelech, M. and W.A. Phillip, *The Future of Seawater Desalination: Energy, Technology, and the Environment*. Science, **2011**. 333(6043): p. 712-717.
3. *Minneapolis Ready for Ultrafiltration*. Available from:  
<http://www.health.state.mn.us/divs/eh/water/com/waterline/featurestories/mpsultrafiltration.htm>.
4. Goosen, M.F.A.; Sablani, S.S.; Al-Hinai, H.; Al-Obeidani, S.; Al-Belushi, R. & Jackson, D. *Fouling of reverse osmosis and ultrafiltration membranes: a critical review*. Separation Science and Technology. **2004**. Vol. 39, No. 10, pp. 2261-2297
5. Eykamp, W., *Microfiltration and ultrafiltration*, in *Membrane Separations Technology: Principles and Applications*, R.D. Noble and S.A. Stern, Editors. **1995**, Elsevier Science: Amsterdam.
6. Asatekin, A., et al., *Anti-fouling ultrafiltration membranes containing polyacrylonitrile-graft-poly (ethylene oxide) comb copolymer additives*. Journal of Membrane Science, **2007**. 298(1-2): p. 136-146.
7. Nguyen, T.; Roddick, A.; Fan, L. *Biofouling of Water Treatment Membranes: A Review of the Underlying Causes, Monitoring techniques and Control Measures*. Membranes. **2012**, 2, 804-840.
8. Guo, W.S., H.H. Ngo, and J.X. Li, *A mini-review on membrane fouling*. Bioresource Technology, **2012**. 122: p. 27-34.
9. Nair, R. R.; Wu, H. A.; Jayaram, P. N.; Grigorieva, I. V.; Geim, A. K. *Unimpeded Permeation of Water through Helium-Leak-Tight Graphene-Based Membranes*. Science **2012**, 335, 442-444.
10. Hu, M.; Mi, B. *Enabling Graphene Oxide Nanosheets as Water Separation Membranes*. Environ. Sci. Technol. **2013**, 47, 3715-3723.
11. Sanchez, V.C., et al., *Biological Interactions of Graphene-Family Nanomaterials: An Interdisciplinary Review*. Chemical Research in Toxicology, **2012**. 25(1): p. 15-34.
12. Akhavan, O. and E. Ghaderi, *Toxicity of Graphene and Graphene Oxide Nanowalls Against Bacteria*. Acs Nano, **2010**. 4(10): p. 5731-5736.
13. Hu, W.B., et al., *Graphene-Based Antibacterial Paper*. Acs Nano, **2010**. 4(7): p. 4317-4323.
14. Perreault, F., M.E. Tousley, and M. Elimelech, *Thin-Film Composite Polyamide Membranes Functionalized with Biocidal Graphene Oxide Nanosheets*. Environmental Science & Technology Letters, **2013**. 1: p. 71-76.

15. Wang, Z.; Yu, H.; Xia, J.; Zhang, F.; Li, F.; Xia, Y.; Li, Y. *Novel GO-Blended PVDF Ultrafiltration Membranes*. *Desalination* **2012**, 299, 50–54.
16. Yu, L.; Zhang, Y.; Zhang, B.; Liu, J.; Zhang, H.; Song, C. *Preparation and Characterization of HPEI-GO/PES Ultrafiltration Membrane with Antifouling and Antibacterial Properties*. *J. Membr. Sci.* **2013**, 447, 452–462.
17. Zhang, J.; Xu, Z.; Shan, M.; Zhou, B.; Li, Y.; Li, B.; Niu, J.; Qian, X. *Synergetic Effects of Oxidized Carbon Nanotubes and Graphene Oxide on Fouling Control and Anti-Fouling Mechanism of Polyvinylidene Fluoride Ultrafiltration Membranes*. *J. Membr. Sci.* **2013**, 448, 81–92.
18. Lee, J.; Chae, H.-R.; Won, Y. J.; Lee, K.; Lee, C.-H.; Lee, H. H.; Kim, I.-C.; Lee, J. *Graphene Oxide Nanoplatelets Composite Membrane with Hydrophilic and Antifouling Properties for Wastewater Treatment*. *J. Membr. Sci.* **2013**, 448, 223–230.
19. Lee, H., et al., *Mussel-inspired surface chemistry for multifunctional coatings*. *Science*, **2007**. 318(5849): p. 426-430.
20. Hwang, S.H., et al., *Poly(vinyl alcohol) Reinforced and Toughened with Poly(dopamine)-Treated Graphene Oxide, and Its Use for Humidity Sensing*. *ACS Nano*, **2014**. 8(7): p. 6739-6747.
21. Zhang, C.; Ou, Y.; Lei, W.; Wan, L.; Ji, J.; Xu, Z. *CuSO<sub>4</sub>/H<sub>2</sub>O<sub>2</sub>-Induced Rapid Deposition of Polydopamine Coatings with High Uniformity and Enhanced Stability*. *Angewandte Chemie Int. Ed.* **2016**, 55, 3054-3057.
22. Hegab, H. M.; ElMekawy, A.; Barclay, T. G.; Michelmore, A.; Zou, L.; Saint, C. P.; Ginic-Markovic, M. *Effective in-situ chemical surface modification of forward osmosis membranes with polydopamine-induced graphene oxide for biofouling mitigation*. *Desalination*. **2016**, 385, 126-137.
23. Tung, V. C.; Allen, M. J.; Yang, Y.; Kaner, R. B. *High-throughput solution processing of large-scale graphene*. *Nat. Nanotechnol.* **2009**, 4(1), 25-29.
24. Zodrow, K.; Brunet, L.; Mahendra, S.; Li, D.; Zhang, A.; Li, Q.; Alvarez, P. J. J. *Polysulfone ultrafiltration membranes impregnated with silver nanoparticles show improved biofouling resistance and virus removal*. *Water Research*. **2009**, 43, 715-723.

2) Publications: none

3) Student support

This grant supported the research of two students: Nathan Karp and Sara BinAhmed

4) Presentations

“Quantifying bacterial adhesion to polymeric membranes by single-cell force spectroscopy”. Sara BinAhmed, Anissa Hasane, and Santiago Romero-Vargas Castrillón. Poster to be presented at the Gordon Conference on Membrane Materials and Processes. July 31 – August 5, 2016, New London, NH

5) Awards

The PI (Romero-Vargas Castrillón) was awarded a 3M Non-tenured during the funding period.

6) Related funding: none

# **Information Transfer Program Introduction**

We did not fund any information transfer projects with our WRII funds.

# USGS Summer Intern Program

None.

| <b>Student Support</b> |                               |                               |                             |                            |              |
|------------------------|-------------------------------|-------------------------------|-----------------------------|----------------------------|--------------|
| <b>Category</b>        | <b>Section 104 Base Grant</b> | <b>Section 104 NCGP Award</b> | <b>NIWR-USGS Internship</b> | <b>Supplemental Awards</b> | <b>Total</b> |
| <b>Undergraduate</b>   | 1                             | 0                             | 0                           | 0                          | 1            |
| <b>Masters</b>         | 4                             | 0                             | 0                           | 0                          | 4            |
| <b>Ph.D.</b>           | 0                             | 0                             | 0                           | 0                          | 0            |
| <b>Post-Doc.</b>       | 0                             | 0                             | 0                           | 0                          | 0            |
| <b>Total</b>           | 5                             | 0                             | 0                           | 0                          | 5            |

## Notable Awards and Achievements

Deborah Swackhamer (former WRC co-director) has been named Chair of the Board of Scientific Counselors (BOSC) of the US EPA. The BOSC provides advice, information, and recommendations to EPA's Office of Research and Development (ORD) on technical and management issues of its research programs by reviewing the quality of on-going science being conducted at the agency. Swackhamer was appointed March 31 by the Administrator for a three year term. Swackhamer has also been appointed to the National Academies of Science Board on Environmental Studies and Toxicology (BEST), one of the NAS permanent boards within the Division of Earth and Life Sciences. BEST organizes and oversees studies of environmental pollution problems affecting human health, human impacts on the environment, and the assessment and management of related risks to human health and the environment. The board's overall mission is to improve the scientific and technical basis for environmental decision making and public understanding of environmental issues. Swackhamer's three year term begins September 2015.

Universities Council on Water Resources (UCOWR) Board of Directors selected Megan Kelly (WRS graduate 2014) as the first place recipient of the 2015 PH.D Dissertation Award in the category of Natural Science and Engineering. Kelly will attend the 2015 UCOWR/NIWR/CUAHSI Conference, Water is Not for Gambling: Utilizing Science to Reduce Uncertainty where she will deliver her dissertation research.

Carlie LaLone (Post/Doctoral Associate, WRC) and a team of EPA researchers were recognized by Environmental Protection Agency administrator Gina McCarthy for developing a software application to inform the use of pathway-based biological data to predict the potential effects of chemicals in a wide range of animal species. This computational tool, titled Sequence Alignment to Predict across Species Susceptibility (SeqAPASS), facilitates rapid and quantitative assessment of the similarities of specific proteins across thousands of species. The research team also includes Gerald Ankley and Daniel L. Villeneuve.

Jim Anderson (former WRC co-director) was awarded a lifetime achievement award from the Minnesota Onsite Wastewater Association (MOWA) at their January 2015 meeting. The award recognizes individuals whose careers in the field of onsite wastewater treatment are exemplary, with outstanding service, dedication and accomplishment for MOWA. Anderson (pictured center) began conducting research and providing education on septic systems in 1971. He and Roger Machmeier started the Onsite Sewage Treatment Program (OSTP) at the University of Minnesota resulting in one of the best education and certification programs in the US. Anderson's soils expertise, combined with Machmeier's engineering knowledge created a program which trains septic system installers, designers, inspectors and service providers. Anderson also helped develop and update Minnesota Rules during over 30 years as chair of the Septic System Advisory Committee.

Anna Baker (MS student) is the 2015 Smith Partners Fellow. The Smith Partners Sustainability Fellowship supports interdisciplinary study for Water Resources graduate students to pursue the connections between sustainable water resources management, economics, and public policy. The Fellowship affirms the University's commitment to sustainability initiatives through cultivation of interdisciplinary problem-solving, collaborative leadership, and public private partnerships.

Brad Gordon (PhD student), Travel grant. Floristic Quality Assessment and the Role of Vegetation in Ravine Erosion in Southern Minnesota. Midwest-Great Lakes Chapter – Society for Ecological Restoration (SER-MWGL) Annual Meeting in Bloomington, Indiana \$300

Cheryl Haines (MS student) Travel grant. The Water Microbiology Conference Chapel Hill, North Carolina. Characterization of the microbiological quality of two non-potable water reuse systems in Minnesota. \$800

Tim Martin (MS student) Travel grant. Ontario Chapter of the American Fisheries Society, Ontario, Canada.  
How Ontario's anglers behave: Insights in the digital age. \$460

Wendy Zhao (PhD student) Travel grant. Association for the Sciences of Limnology and Oceanography  
Summer Meeting June 5-10, Santa Fe, NM, Testing the theory of Island Biogeography in freshwater bacterial  
communities and Dynamics of water and particle associated bacterial communities in near shore Lake  
Superior and the Duluth-Superior Harbor \$1000